

Abstract

Observations suggest tropical convection intensifies when aerosol concentrations enhance, but quantitative estimations of this effect remain highly uncertain. Leading theories for explaining the influence of aerosol concentrations on tropical convection are based on the dynamical response of convection to changes in cloud microphysics, neglecting possible changes in the environment. In recent years, global convection-permitting models (GCPM) have been developed to circumvent problems arising from imposing artificial scale separation on physical processes associated with deep convection. Here, we use a GCPM to investigate how enhanced concentrations of aerosols that act as cloud condensate nuclei (CCN) impact tropical convection features by modulating the convection-circulation interaction. Results from a pair of idealized non-rotating radiative-convective equilibrium simulations show that the enhanced CCN concentration leads to weaker large-scale circulation, the closeness of deep convective systems to the moist cluster edges, and more mid-level cloud water at an equilibrium state in which convective self-aggregation occurred. Correspondingly, the enhanced CCN concentration modulates how the diabatic processes that support or oppose convective aggregation maintain the aggregated state at equilibrium. Overall, the enhanced CCN concentration facilitates the development of deep convection in a drier environment but reduces the large-scale instability and the convection intensity. Our results emphasize the importance of allowing atmospheric phenomena to evolve continuously across spatial and temporal scales in simulations when investigating the response of tropical convection to changes in cloud microphysics.

Plain Language Summary

How does air pollution affect thunderstorm intensity over the tropical ocean? Past studies have proposed different opinions but generally neglect the interplay between the development of thunderstorms and the long-range movement of air that redistributes the Earth's thermal energy and moisture. Here, we address this question by investigating results from idealized numerical experiments in which the global domain is used to simultaneously simulate the response of individual thunderstorms and large-scale air motion to pollution. We found that pollution makes the thunderstorms keep less moisture in their surroundings, limiting the intensity of thunderstorms and weakening the large-scale air motion that supplies moisture to thunderstorms. Our results suggest that the interplay between the development of thunderstorms and the long-range movement of air is crucial in determining the effects of pollution in the tropical atmosphere.

1 Introduction

Tropical moist convection has long been recognized as a critical role in the global climate system (Arakawa, 2004; Hartmann et al., 2001). Various meteorological phenomena in the tropics are associated with the interaction between moist convection and atmospheric circulation, such as mesoscale convective systems (Houze, 2004) and convectively coupled waves (Kiladis et al., 2009; Lau & Lau, 1990). A deeper understanding of convection-circulation interaction across temporal and spatial scales is important for improving global climate predictions and forecasts of extreme precipitation events (Tomassini, 2020).

In recent years, several numerical modeling groups have developed global convection-permitting models (GCPMs) that explicitly simulate deep moist convection on the global domain to circumvent problems arising from parameterizations that presumably determine how circulations govern moist convection or how moist convection drives circulations (Caldwell et al., 2021; Hohenegger et al., 2023; Stevens et al., 2019). Interestingly, while the GCPMs capture basic aspects of the general circulation, they produce a diverse range of tropical convective systems (Feng et al., 2023; Su et al., 2022). For example, the distribution of tropical cloud modes varies greatly across the models (Nugent

65 et al., 2022; Roh et al., 2021; Turbeville et al., 2022). The diversity in tropical convec-
66 tion features among the GCPMs has not been fully understood. One of the challenges
67 to closing the knowledge gap is that the response of tropical convection and the large-
68 scale circulation to any model treatment of subgrid-scale physical process (e.g., turbu-
69 lence, microphysics) or natural and anthropogenic forcing are coupled throughout sim-
70 ulations. Hence, identifying the sensitivity of tropical convection-circulation to individ-
71 ual components or processes in the global climate system is critical to understanding the
72 cause of the diverse tropical convection features among the GCPMs. Observations sug-
73 gest that enhanced aerosol concentrations that arise from human activities and natural
74 sources can substantially influence updrafts of tropical deep convection (Andreae et al.,
75 2004; Koren et al., 2008; Niu & Li, 2012; Pan et al., 2021; Storer et al., 2014), but lead-
76 ing theories for explaining the influence neglects possible changes in the environment through
77 convection-circulation interaction. In this study, we aim to investigate the impact of en-
78 hanced aerosol concentrations on tropical convection features using a GCPM.

79 By acting as cloud condensate nuclei (CCN) or ice nuclei (IN), aerosols change cloud
80 properties by influencing cloud microphysics and dynamics, meanwhile influencing cloud-
81 radiation feedbacks (i.e., aerosol indirect effects (AIEs); see reviews of Fan et al. (2016)
82 and Tao et al. (2012)). However, the underlying mechanisms of how the updrafts are in-
83 fluenced remain elusive and are often debated (Fan et al., 2018; Fan & Khain, 2021; Grabowski
84 & Morrison, 2020, 2021; Igel & van den Heever, 2021; J. M. Peters et al., 2023; Romps
85 et al., 2023). A particular challenge of understanding AIEs using observations is that the
86 observed aerosol concentrations in the environments of tropical deep convection often
87 covary with other meteorological factors, such as convective available potential energy
88 and vertical wind shear (Grabowski, 2018; Nishant & Sherwood, 2017; Varble, 2018), and
89 the influences of meteorological and aerosol variability are difficult to disentangle from
90 one another. Further, there is evidence from simulations that AIEs on deep convection
91 vary as a function of meteorological conditions such as shear and humidity (Fan et al.,
92 2009; van den Heever & Cotton, 2007; Khain et al., 2008; Koren et al., 2010; Lebo, 2018),
93 which further complicates our ability to isolate the aerosol effects from other meteoro-
94 logical processes.

95 To take into account the interaction between tropical convection and the surround-
96 ing environment, Abbott and Cronin (2021) carried out simulations using a small do-
97 main ($128 \times 128 \text{ km}^2$) three-dimension cloud-resolving model (3-D CRM) with parame-
98 terized large-scale dynamics under the weak temperature gradient (WTG) approxima-
99 tion (Sobel et al., 2001). They suggested that enhanced aerosol concentrations produce
100 clouds that mix more condensed water into the surrounding air. This enhances the en-
101 vironment favorably for subsequent convection by moistening the free troposphere and
102 reducing the deleterious effects of entrainment. The humidity-entrainment mechanism
103 they proposed is distinct from past work, which linked stronger updrafts with latent heat
104 released by cloud condensation (Fan et al., 2018) or freezing (Rosenfeld et al., 2008) in-
105 dependently from possible changes in the environment. Using a similar modeling frame-
106 work but under a different large-scale flow regime, Anber et al. (2019) found a contrast-
107 ing result. In their simulations, convection and mean precipitation get weaker when the
108 CCN concentration increases. They suggested that the changes are associated with the
109 modulation of the coupling between convective processes and large-scale motions, which
110 reduces surface enthalpy fluxes, rather than the changes in microphysical properties.

111 In CRM simulations that use a large domain for explicitly simulating the large-scale
112 circulation between convecting and nonconvecting regions, results of AIEs on tropical
113 convection have not reached a consensus as well. For example, van den Heever et al. (2011)
114 found a weak response of the large-scale organization of convection and the domain-averaged
115 precipitation to enhanced CCN concentrations in their 2-D CRM simulations (10000 km)
116 configured in non-rotating radiative-convective equilibrium (RCE; Manabe & Strickler,
117 1964) with a fixed sea surface temperature (SST). They suggested that AIEs on the three

118 tropical cloud modes are quite significant in magnitude and often opposite in sign, off-
 119 setting each other, thus producing a weak domain-wide response. In contrast, Beydoun
 120 and Hoose (2019) found a comparatively large decrease in domain-averaged precipita-
 121 tion with enhanced CCN concentrations in their RCE simulations of a channel-shaped
 122 (2000x120 km²) 3-D CRM. They suggested that enhanced CCN concentrations weaken
 123 the large-scale organization of convection, leading to decreased domain-averaged precip-
 124 itation. As discussed in Beydoun and Hoose (2019), the discrepancy between the results
 125 of the two studies may be caused by the difference in how the aerosol changes are im-
 126 posed and the difference in model setup of domain geometry. Previous studies of RCE
 127 simulations found that the size of the simulation domain impacts the mechanisms that
 128 trigger and maintain the large-scale organization of convection (Jeevanjee & Romps, 2013;
 129 C. J. Muller & Held, 2012; Patrizio & Randall, 2019). A horizontal scale of model do-
 130 main larger than 5000 km was suggested to be large enough to represent the natural scale
 131 of large-scale organization of convection and reach convergence of equilibrium states in
 132 simulations with different domain sizes (Matsugishi & Satoh, 2022; Yanase et al., 2022).

133 The goal of this study is to investigate how enhanced CCN concentration impacts
 134 tropical convection features through modulating the convection-circulation interaction
 135 using a GCPM that simultaneously simulates the dynamical response of tropical deep
 136 convection to changes in cloud microphysics and allows the large-scale organization of
 137 convection to naturally develop without artificial constraints due to domain size or shape.
 138 Idealized non-rotating RCE simulations with different scenarios of CCN concentration
 139 were carried out using the Central Weather Bureau Global Forecast System (CWBGFS;
 140 Su et al., 2021a).

141 Simulations configured in RCE have been extensively used to investigate feedbacks
 142 among clouds, environmental moisture, radiation, and precipitation (Bretherton et al.,
 143 2005; Coppin & Bony, 2015; Cronin & Wing, 2017; K. Emanuel et al., 2014; Holloway
 144 & Woolnough, 2016; Pendergrass et al., 2016; Popke et al., 2013; Singh & O’Gorman,
 145 2013, 2015; Wing & Emanuel, 2014; Wing et al., 2020), providing an ideal experimen-
 146 tal setting for our study. Previous studies found that convection in simulations config-
 147 ured in RCE can spontaneously self-organize into one or more moist ascending clusters
 148 surrounded by dry subsiding convection-free areas (convective self-aggregation (CSA);
 149 C. Muller et al., 2022; Wing et al., 2017). The occurrence of CSA changes the climate
 150 mean state dramatically (i.e., atmospheric heating and drying) and gives rise to the large-
 151 scale organization of convection that develops in line with the large-scale circulation. As
 152 will be shown later in this paper, CSA occurs in both of our simulations, but the degree
 153 of large-scale organization of convection changes with the enhancement of CCN concen-
 154 tration. We note that the terminologies of large-scale organization of convection and ag-
 155 gregation are used interchangeably in this paper, as they represent the same concept,
 156 at least in the scope of this study. The following section introduces more details about
 157 the model and our experiment design. Section 3 describes the results of the simulations
 158 when a statistical equilibrium is reached, and the summary and discussion are presented
 159 in section 4.

160 2 Model Description and Experiment Design

161 The Central Weather Bureau Global Forecast System (CWBGFS; Su et al., 2021a)
 162 is a global convection-permitting model that run at the horizontal resolution of around
 163 15 km. Deep convection in the CWBGFS is represented by the unified relaxed Arakawa-
 164 Schubert scheme (URAS; Su et al., 2021b) in which the representation transitions from
 165 the parameterization to the explicit simulation as the diagnosed convective updraft frac-
 166 tion increases (Arakawa & Wu, 2013; Wu & Arakawa, 2014). Hence, the CWBGFS with
 167 the URAS can explicitly but efficiently simulate deep convection and the associated convection-
 168 circulation interaction on a global scale. The model partially resolves circulations in or-

169 ganized convective systems and reproduces the observed feature of convective systems
 170 that stronger extreme precipitation occurs in horizontally larger systems (Su et al., 2022).

171 In the CWBGFS, cloud microphysical processes, including cloud droplet activa-
 172 tion, are represented by the two-moment Predicted Particle Properties bulk microphysics
 173 scheme (P3; Morrison & Milbrandt, 2015). Since the convective updraft fraction increases
 174 with updraft velocity so that the representation of deep convection transitions to explicit
 175 simulation as updraft enhances (Su et al., 2021b), we assume that taking cloud-aerosol
 176 interaction into account in the cloud model of URAS makes a small impact on the trop-
 177 ical convection features and will not change the conclusion of this study. On average, more
 178 than 93 % of precipitation is produced by explicitly simulated convection through the
 179 P3 scheme over precipitation events stronger than 5 mm h^{-1} . In the version of the P3
 180 scheme used in this study, the aerosol is specified as a lognormal size distribution with
 181 a constant background aerosol concentration and mean size of $0.05 \mu\text{m}$, consisting of am-
 182 monium sulfate. The number of activated CCN is a function of supersaturation given
 183 by Morrison and Grabowski (2007, 2008). The rest of the descriptions regarding physics
 184 suites and the dynamic core of the CWBGFS can be found in Su et al. (2021a).

185 We carried out two idealized non-rotating aqua-planet simulations configured in
 186 RCE with different constant background aerosol concentrations using the CWBGFS. Set-
 187 ting the background aerosol concentration as a constant provides us the simplest scenario
 188 for examining the changes in convection variability over space and the pattern of large-
 189 scale circulation with aerosol concentrations. As this study focuses on the AIEs, aerosols
 190 in the microphysics scheme do not interact with radiation. The current study sets the
 191 constant background aerosol concentration to $3 \times 10^8 \text{ kg}^{-1}$ (pristine run) and $3 \times 10^{10} \text{ kg}^{-1}$
 192 (polluted run) throughout the simulation, respectively. The scenarios here are referred
 193 to the marine environment (Andreae, 2009) and the urban environment (Chang et al.,
 194 2021). Previous studies suggested that tropical mean precipitation does not change with
 195 the enhancement of CCN concentration monotonically (van den Heever et al., 2011; Storer
 196 & van den Heever, 2013). Experiments with more diverse polluted scenarios will be car-
 197 ried out in the future.

198 The pristine run and the polluted run are initialized with the same analytic sound-
 199 ing (Wing et al., 2018) that approximates the moist tropical sounding of Dunion (2011),
 200 and the initial horizontal winds are set to zero. The initial surface pressure of all grid
 201 columns is 1014.8 hPa. The incoming solar radiation (409.6 W m^{-2}), the SST (300 K),
 202 and the surface albedo (0.07) are spatially uniform and remain constant in time. The
 203 simulations are run for 120 days, and the random perturbation of temperature from 0.1
 204 to 0.02 K is added to the five lowest model levels in the first 20 days to speed up con-
 205 vection initiation. In the following section, we analyze results from day 100 to 120 when
 206 a statistical equilibrium state is met (Fig. S1) using hourly outputs. We note that the
 207 two runs may experience different transition processes to arrive at their equilibrium state,
 208 and a slow-phase oscillation of the global energy budget could exist. We assume that the
 209 probable presence of such a slow-phase oscillation would not change the conclusion of
 210 this study because the energy budget in both runs does not exhibit an obvious chang-
 211 ing trend in the last 50 days of integration (Fig. S1).

212 3 Results

213 The RCE simulations in this study have typical features of CSA shown in the global
 214 model simulations of the RCE model intercomparison project (Wing et al., 2018, 2020),
 215 showing drying of the atmosphere and enhancement of spatial moisture variance. As con-
 216 vection self-organizing into multiple moist clusters, the global average of CWV decreases
 217 from the initial condition of 49.93 mm to the equilibrium state (day 100-120) of 29.96
 218 mm in the pristine run and 29.73 mm in the polluted run (Fig. S1). Fig. 1 shows the
 219 spatial distribution of CWV at day 110. Both runs exhibit a high heterogeneity of CWV

220 within moist clusters, which is coupled to convection. The pristine run has notably more
 221 occurrence of high CWV events (>60 mm). One can see that the CWV hotspots (>60
 222 mm) in the pristine run occur over regions closer to the geometric center of each moist
 223 cluster than they do in the polluted run. We find that this particular feature may play
 224 an important role in the convection-circulation interaction, which will be investigated
 225 later in this paper.

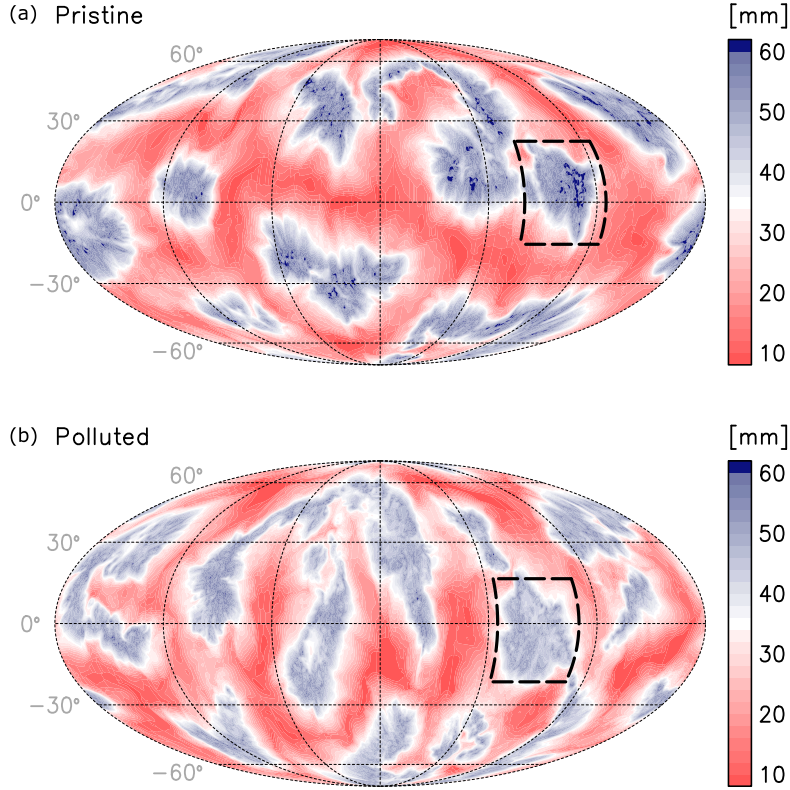


Figure 1. Spatial distribution of CWV at day 110 of the pristine run (a) and the polluted run (b).

226 At the equilibrium state, both runs exhibit a bimodal probability distribution of
 227 CWV (Fig. 2). The bimodality is associated with the presence of an aggregated state
 228 of convection (Tsai & Wu, 2017). The difference in CWV between the two local max-
 229 ima of the bimodality is smaller in the polluted run, suggesting that the aggregated state
 230 in the polluted run is maintained by weaker large-scale circulation, and the aggregated
 231 state consists of drier moist clusters and wetter dry regions. Associated with the weak-
 232 ened large-scale circulation, the global averages of outward OLR and precipitation in-
 233 tensity at the equilibrium state are lower in the polluted run (287.45 W m^{-2} , 0.167 mm h^{-1})
 234 than that in the pristine run (292.43 W m^{-2} , 0.174 mm h^{-1}). The polluted run has
 235 a colder temperature profile compared to that in the pristine run, with the largest dif-
 236 ference of 1.7 K occurring at 200 hPa (Fig. S2). Meanwhile, the polluted run has the
 237 lower spatial variance of vertically integrated frozen moist static energy (FMSE) (1.03×10^{15}
 238 $\text{J}^2 \text{m}^{-4}$) compared to that in the pristine run ($1.32 \times 10^{15} \text{ J}^2 \text{m}^{-4}$). The FMSE has been used
 239 in studies of CSA to quantify the degree of aggregation

$$h = C_p T + gz + L_v q_v - L_f q_{ice}, \quad (1)$$

240 where C_p is the specific heat capacity of air, T is temperature, g is the gravitational ac-
 241 celeration, z is geopotential height, L_v is the latent heat of vaporization, q_v is the wa-
 242 ter vapor mixing ratio, L_f is the latent heat of fusion, and q_{ice} represents all ice phase
 243 condensates. During our analysis period, the variation in the spatial variance of verti-
 244 cally integrated FMSE with time in both runs is much less than the difference between
 245 the two runs (Fig. S3).

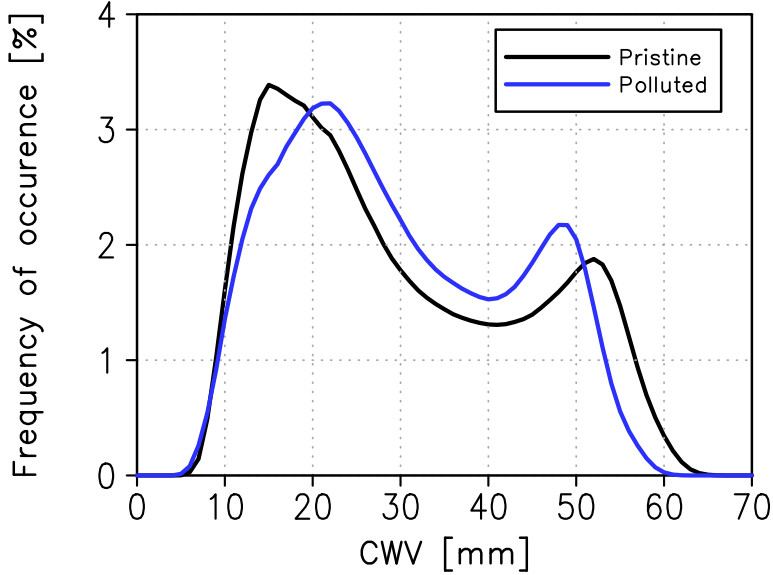


Figure 2. Probability distribution of CWV from days 100 to 120.

246 To identify the changes in energy transport between moist clusters and dry regions
 247 caused by pollution, we use the stream function on moisture space (Arnold & Putman,
 248 2018)

$$\Psi_i(p) = \Psi_{i-1}(p) + \omega_i(p), \quad (2)$$

249 where p is pressure and ω_i is the pressure velocity averaged over the i^{th} CWV bin. Both
 250 runs in this study exhibit a shallow circulation, which transports moist static energy (MSE)
 251 upgradient, maintaining the large-scale organization of convection (Arnold & Putman,
 252 2018; C. Muller et al., 2022), and a deep circulation, which exports MSE from moist as-
 253 cending regions (Fig. 3a and 3b). While the deep circulation is directly driven by deep
 254 convection, the differential radiative cooling between moist clusters and dry regions (Fig.
 255 3c and Fig. 3d) associated with the vertical gradients of relative humidity and clouds
 256 over dry regions (Fig. 3e and Fig. 3f) is believed to be one of the factors that drive shal-
 257 low circulation in RCE simulations (C. J. Muller & Held, 2012). In general, the patterns
 258 of energy transport in the two runs are very much alike. The polluted run has the larger
 259 stream function at the upper free troposphere (300-400 hPa) compared to that in the
 260 pristine run (Fig. 3a and 3b), which suggests that the mean ascending motions are dis-
 261 tributed wider in the moisture space when the environment is more polluted. However,
 262 the difference in the density of the stream function contours over there between the two
 263 runs is marginal. The difference in the low-level subsidence over dry regions between the
 264 two runs is also hard to be identified through Fig. 3a and 3b. We note that the polluted

265 run has a higher cloud water mixing ratio over grid columns with CWV more than the
 266 70th percentile compared to that in the pristine run, which is likely caused by enhanced
 267 cloud drop activation due to pollution.

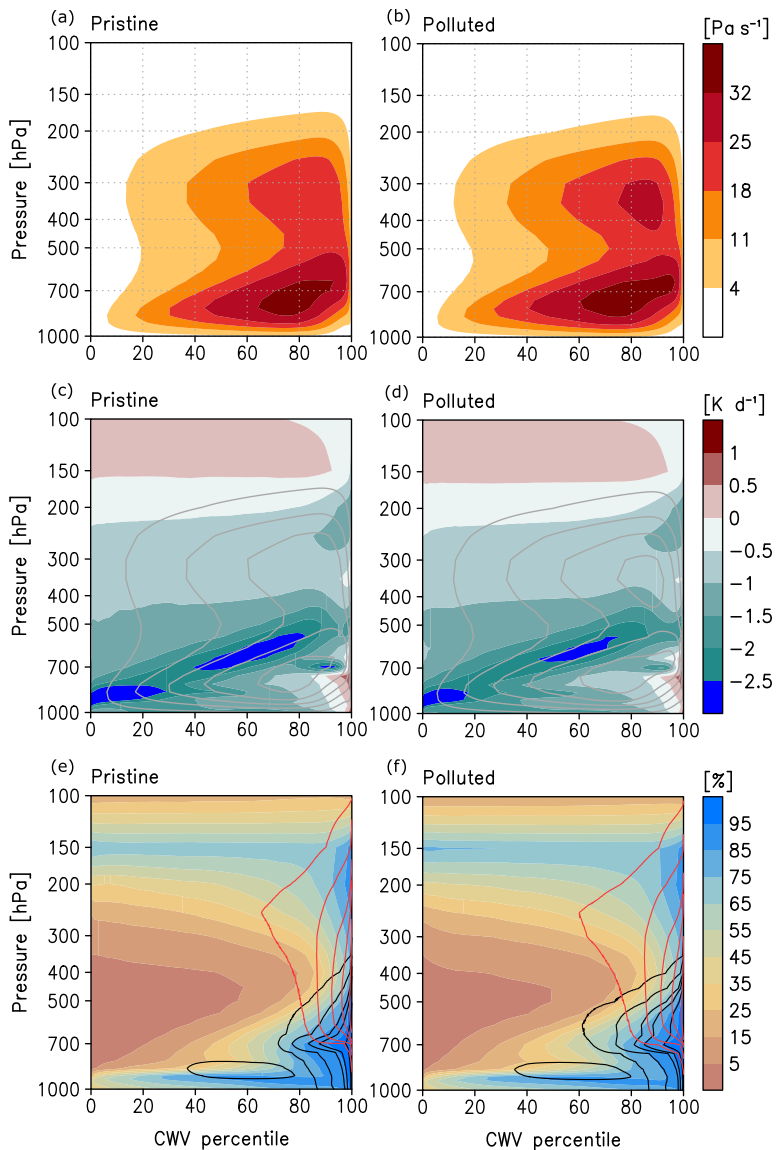


Figure 3. Vertical profiles of stream function (shaded) (a,b), radiative heating rate (shaded) (c,d), relative humidity (shaded), and cloud water (black) and cloud ice (red) mixing ratio contoured at 0.001, 0.01, 0.05, 0.1, 0.3 g kg^{-1} (e,f) conditionally sampled by CWV in the pristine run (left column) and the polluted run (right column) from day 100 to 120. The stream function in a,b is shown as contours in c,d.

268 As the stream function on moisture space does not represent physical horizontal
 269 flows, we further analyze the large-scale circulation on physical space in each run. We
 270 define moist clusters as contiguous grid columns with CWV $>75^{\text{th}}$ percentile in horizontal
 271 directions and dry regions as areas not defined as moist clusters. The 75th percentile
 272 of CWV is 42.34 mm in the pristine run and 40.75 mm in the polluted run. For each grid

273 column, the distance to the edge of the nearest moist cluster with a spatial scale larger
 274 than 500 km (defined as the square root of horizontal area) is calculated. Horizontal winds
 275 at each vertical level are then projected to the direction pointing to the nearest edge and
 276 conditionally sampled by the distance to the edge. We neglect moist clusters smaller than
 277 500 km because they are rare events that quickly dissipate or merge into larger moist
 278 clusters. The distance-binned projected horizontal wind speed and vertical velocity are
 279 shown in Fig. 4a and 4b. Negative distance values refer to areas inside the moist clus-
 280 ters as the distance is multiplied by -1 for grid columns belong a moist cluster.

281 The plot makes it clear that the polluted run has a weaker low-level inflow (below
 282 850 hPa) from dry regions to moist clusters and a weaker high-level outflow (above 300
 283 hPa) compared to those in the pristine run. Over moist clusters, the mean ascending mo-
 284 tions are weaker and closer to the edge in the polluted run, but the difference in the max-
 285 imum magnitude of the mean updrafts between the two runs is subtle. The mean CWV
 286 is homogeneous in regions within moist clusters but away from the edge ($d < -500 \text{ km}$, $d =$
 287 *distance to the nearest edge*) (Fig. 5a), while the distribution of the mean precipita-
 288 tion intensity is maximized near the edge (Fig. 5b) reflecting the distribution of the mean
 289 ascending motions. We speculate that the imprint of the changes in deep convection fea-
 290 tures caused by pollution on large-scale circulation is illustrated by analysis based on phys-
 291 ical space rather than moisture space because the impact of pollution on deep convec-
 292 tion intensity does not enhance or reduce monotonically to the increase in CWV.

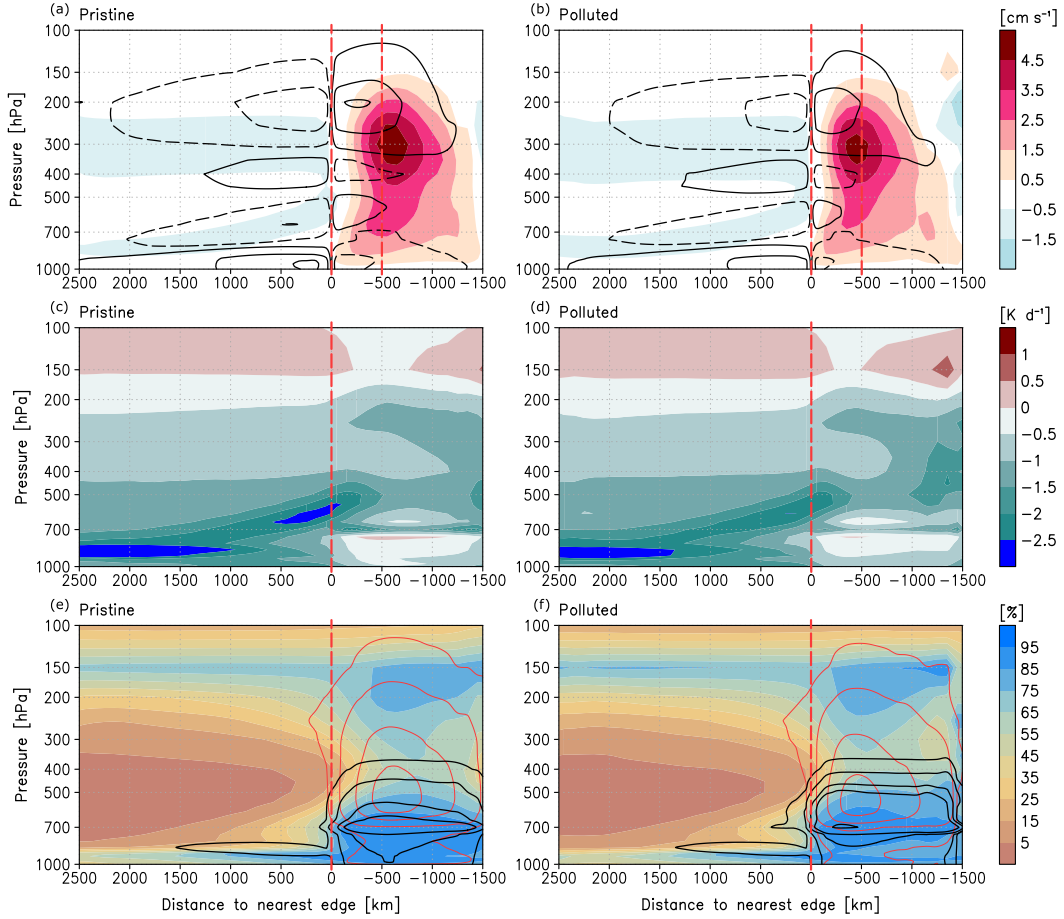


Figure 4. Vertical profiles of projected horizontal wind speed (contours at 0.5, 2.5, 4.5 m s^{-1}), vertical velocity (shaded) (a,b), radiative heating rate (shaded) (c,d), relative humidity (shaded), and cloud water (black) and cloud ice (red) mixing ratio contoured at 0.001, 0.01, 0.05, 0.1, 0.3 g kg^{-1} (e,f) conditionally sampled by the distance to the nearest edge in the pristine run (left column) and the polluted run (right column) from day 100 to 120. Projected horizontal wind pointing toward (away) the edge is shown by solid (dashed) contours. Negative distance values refer to areas inside the moist clusters

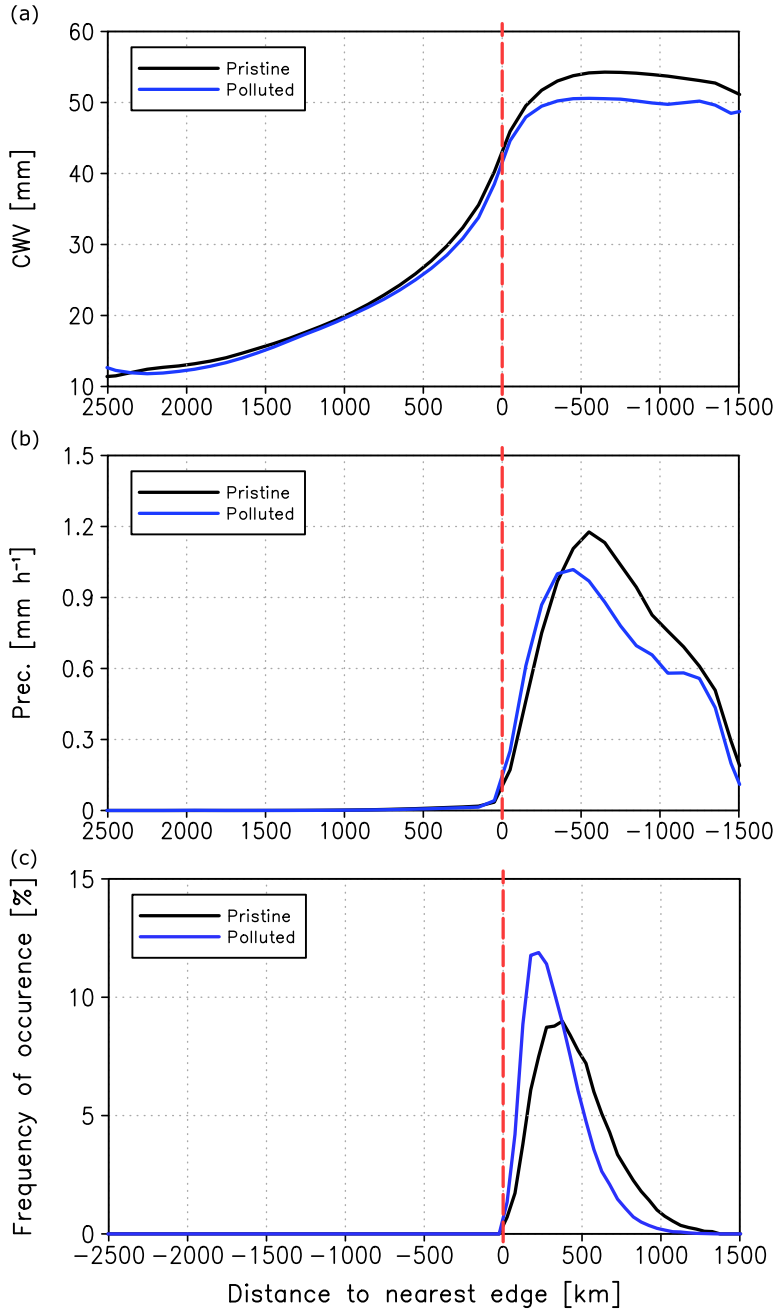


Figure 5. CWV (a), precipitation intensity (b), and the occurrence of explicitly simulated convection objects (c) conditionally sampled by the distance to the nearest edge from day 100 to 120.

293 We zoom in to one of the moist clusters to showcase the difference in the spatial
 294 distribution of convection between the two runs. Fig. 6a-d show the snapshots of vertical
 295 velocity at 500 hPa on top of CWV and precipitation intensity within the dashed
 296 rectangle shown in Fig. 1. In the polluted run, explicitly simulated convection develops
 297 over regions closer to the edge compared to that in the pristine run. This inference is
 298 further supported by the analysis of the distance from the geometric center of each convection
 299 object to its nearest edge (Fig. 5c), in which a convection object is defined as

300 contiguous grid cells with vertical velocity at 500 hPa $>0.1 \text{ m s}^{-1}$. In both runs, the high-
 301 est probability of convection object occurrence is located at $-500 < d < 0 \text{ km}$.

302 Why are updrafts, especially those in the polluted run, preferably take place close
 303 to the edge? Intensification of tropical deep convection at the edge of convectively ac-
 304 tive regions has been identified by previous studies of observations (Mapes et al., 2018)
 305 and idealized RCE simulations (Becker et al., 2018; Windmiller & Hohenegger, 2019).
 306 Windmiller and Hohenegger (2019) proposed that the cause for the edge intensification
 307 is dynamical lifting by strong surface convergence that results from two opposing flows:
 308 a low-level inflow from dry regions to moist clusters and the propagation of continuously
 309 forming cold pools within moist clusters. Fig. 6e,f show the spatial distribution of the
 310 divergence field at 1000 hPa in our simulations. We can see the near-surface divergence
 311 collocates with updrafts, and strong near-surface convergence can be seen at regions be-
 312 tween the edge and the existing updrafts. We speculate that the mechanism proposed
 313 by Windmiller and Hohenegger (2019) explains the edge intensification in our simula-
 314 tions, and the weaker low-level inflow in the polluted run may be one of the factors to
 315 polluted updrafts being closer to the edge. As will be shown later in this paper, pollu-
 316 tion has a larger impact on the probability distribution of near-surface inflow than its
 317 impact on the probability distribution of the estimated cold pool propagation velocity
 318 in our simulations.

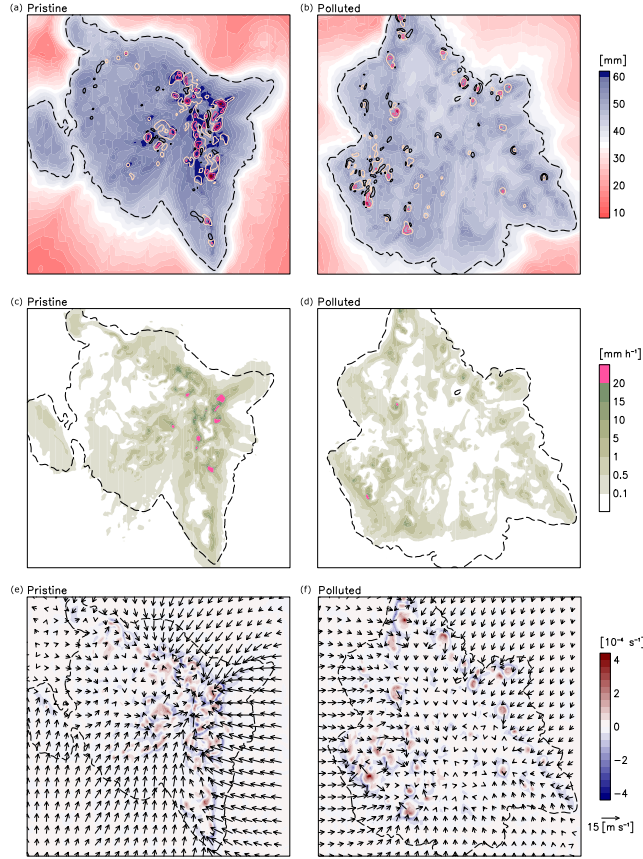


Figure 6. Spatial distribution of CWV, updraft velocity at 500 hPa (red scale, contoured at 0.1, 0.5, 1, 1.5 m s^{-1}), downdraft velocity at 500 hPa (black solid, contoured at 0.1 m s^{-1}) (a,b), precipitation intensity (c,d), and divergence field at 1000 hPa at day 110 of the pristine run (left column) and the polluted run (right column). The edge of the moist cluster (i.e., the 75th percentile of CWV) is demonstrated by black dashed lines.

Table 1. Spatial and temporal mean of each term in the right-hand side of eq.3

$[day^{-1}]$	Pristine moist clusters	Pristine dry regions	Polluted moist clusters	Polluted dry regions
Advection	-0.060	-0.007	-0.097	-0.004
SEF	-0.069	0.001	-0.045	-0.005
NetLW	0.065	-0.004	0.087	-0.001
NetSW	0.057	0.015	0.049	0.016

319 The distance-binned radiative heating rate, relative humidity, and hydrometeors
320 mixing ratio over dry regions (Fig. 4c-f) resemble the CWV-binned results (Fig. 3c-f),
321 except in physical space it is apparent that the polluted run has more mid-level (700 hPa)
322 cloud water over the regions close to the edge ($0 < d < 500 km$) than the pristine run
323 does. The level of the cloud water coincides with the level of the outflow of shallow cir-
324 culation from moist clusters, suggesting that polluted moist clusters export more cloud
325 water to the dry regions than their pristine counterparts, and pollution may modulate
326 the role of shallow circulation in maintaining the aggregated state.

327 To investigate the modulation of the diabatic processes that support or oppose con-
328 vective aggregation by pollution, we analyze a budget of the spatial variance of FMSE
329 at the equilibrium state as a quantitative account of the large-scale organization of con-
330 vection following (Wing & Emanuel, 2014). The FMSE is a desirable diagnostic because
331 vertically integrated FMSE can only be changed by radiation, surface fluxes, and advec-
332 tion. A process that contributes to the FMSE variance supports aggregation, and a pro-
333 cess that reduces the FMSE variance opposes aggregation.

334 The budget equation of vertically integrated FMSE is given by eq. (9) in Wing and
335 Emanuel (2014)

$$\frac{1}{2}\partial_t \hat{h}'^2 = -\hat{h}'\nabla_h \cdot \widehat{\vec{u}h} + \hat{h}'NetLW' + \hat{h}'NetSW' + \hat{h}'SEF', \quad (3)$$

336 where primes denote anomalies relative to the spatial mean and hats denote the mass-
337 weighted column integral. \hat{h}' is the anomaly of vertically integrated FMSE, $\nabla_h \cdot \widehat{\vec{u}h}$ rep-
338 represents the horizontal transport, $NetLW'$ is the anomaly of column longwave conver-
339 gence, $NetSW'$ is the anomaly of column shortwave convergence, and SEF' is the anomaly
340 of surface enthalpy fluxes. Each term in eq. (3) is calculated for each grid column us-
341 ing hourly outputs. We calculate the horizontal convergence term, the first term on the
342 right-hand side, as a residual from the rest of the terms in eq. (3) following previous stud-
343 ies that have done FMSE budget calculations (Bretherton et al., 2005; C. J. Muller &
344 Held, 2012; Wing & Emanuel, 2014). We arrive at an equation for the spatial variance
345 by normalizing each term by the instantaneous horizontal mean of \hat{h}'^2 . We then aver-
346 age each term over the analysis period (day 100-120) over moist clusters and dry regions,
347 respectively. The result of the calculation is demonstrated in Table 1.

348 The diabatic processes over moist clusters are more dominant in maintaining the
349 aggregated state than they do over dry regions, as Table 1 shows that the terms over moist
350 clusters are much greater than those over dry regions in both runs. Hence, we focus on
351 the diabatic processes over moist clusters in the following analysis. We can see that ad-
352 vection and surface enthalpy fluxes are the terms that oppose aggregation, while the ra-
353 diation terms support aggregation. The negative value of the advection term indicates
354 that the deep circulation, which represents a positive gross moist stability (Neelin & Held,
355 1987), governs the advection term so that the overall large-scale circulation tends to sta-
356 bilize moist clusters. The polluted run has a greater negative value of the advection term
357 compared to that in the pristine run. As the aforementioned results have demonstrated

358 that the polluted run has weaker deep circulation, we suspect that the greater negative
 359 value of the advection term results from the reduction in the upgradient energy trans-
 360 port by shallow circulation. The primary factor of the reduction appears to be the greater
 361 export of cloud water at mid-level in the polluted run, as cloud water is implicitly taken
 362 into account by FMSE.

363 The negative value of surface enthalpy fluxes term in both runs suggests that the
 364 negative air-sea enthalpy disequilibrium feedback (Wing & Emanuel, 2014) overcomes
 365 the positive wind-induced surface heat exchange (WISHE; K. A. Emanuel, 1987) feed-
 366 back in our model. Because our simulations use a fixed, uniform SST, the air-sea enthalpy
 367 disequilibrium depends on the near-surface water vapor mixing ratio. In the polluted run,
 368 the less column moisture over moist clusters may be responsible for the less negative value
 369 of the surface enthalpy fluxes term compared to the pristine run. As for the radiation
 370 terms, pollution leads to a greater value of the longwave term and a lower value of the
 371 shortwave term, of which more cloud cover emitting less energy outward and less col-
 372 umn moisture absorbing less energy may be the primary factor, respectively. Overall,
 373 the budget analysis demonstrates that the modulation of how the diabatic processes that
 374 support or oppose convective aggregation maintain the aggregated state at equilibrium
 375 is consistent with the other results in this study. To further quantify the cause and ef-
 376 fect of a certain process associated with AIEs, a different experiment setup with a fo-
 377 cus on the transition between equilibrium states is necessary but out of the scope of this
 378 study.

379 The current result demonstrates that pollution modulates the relative role of shal-
 380 low circulation in the overall energy transport under the equilibrium state with weaker
 381 large-scale circulation. The enhancement in the mid-level cloud water export from moist
 382 clusters appears to be a key factor of the modulation. The aforementioned result implies
 383 that the enhancement may be related to the closeness of the convection to the moist clus-
 384 ter edges.

385 The heterogeneity of convection over space in moist clusters illustrated in Fig. 1
 386 and Fig. 6 suggests that isolating deep convection from the environment is necessary to
 387 elucidate the difference in bulk attributes of convection features between the polluted
 388 and the pristine run. We use the convective system identification method following Feng
 389 et al. (2019), defining cold cloud systems (CCSs) as contiguous grid cells with bright-
 390 ness temperature $T_b < 241 K$. The OLR in our model outputs is converted to T_b fol-
 391 lowing Yang and Slingo (2001). Fig.7 shows the mean vertical profiles of vertical veloc-
 392 ity and hydrometeors mixing ratio within CCSs and the mean vertical profile of cloud
 393 water mixing ratio over regions in moist clusters but not defined as a CCS. We can see
 394 that the CCSs have top-heavy vertical profiles in both runs, while the polluted run has
 395 weaker mean vertical velocity (Fig. 7a). The weaker vertical velocities in the polluted
 396 run imply smaller condensation and deposition rates and lesser buoyancy production aloft.
 397 Consistent with this idea, there is less cloud ice within the polluted run (Fig. 7b). On
 398 the other hand, the enhanced CCN concentration results in a larger fraction of liquid oc-
 399 ccurring as cloud water (rather than rain). The polluted run has a cloud water mixing
 400 ratio more than twice that of the pristine run over both the CCSs and the other regions
 401 in moist clusters (Fig. 7c-d). The higher cloud water mixing ratio over regions outside
 402 of CCSs in the polluted run compared to that in the pristine run implies that pollution
 403 may lead to an increase in mid-level static stability, which promotes detrainment of cloud
 404 water into the environment (Johnson et al., 1999; Posselt et al., 2008).

405 The warm rain amount in the polluted run is less than that in the pristine run (Fig.
 406 7e), which is an expected result (Rosenfeld, 1999). The polluted run has more falling rimed
 407 ice at the mid-to-low level (400-850 hPa) and the near-surface (Fig. 7f), showing that
 408 the partition between cold rain and warm rain may be different between the two runs.
 409 However, the impact of pollution on the mixed-phase microphysical processes can not

410 be isolated from the other controlling factors in our simulations because the two runs
 411 have contrasting environmental conditions.

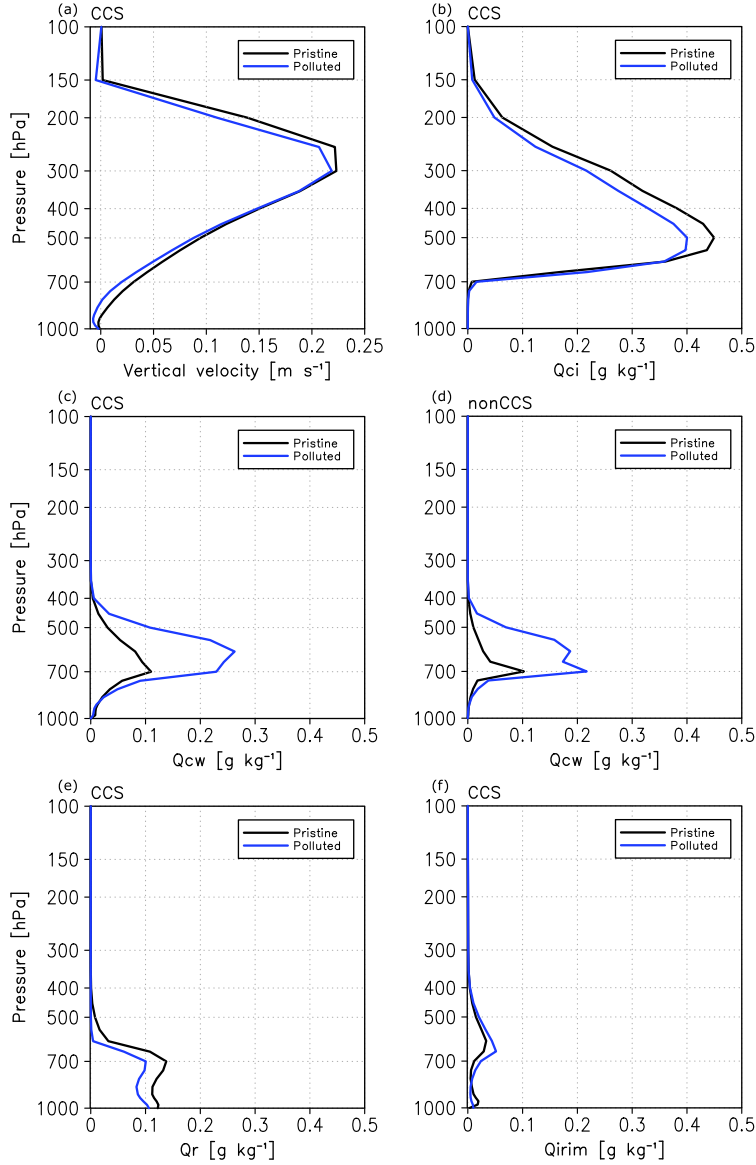


Figure 7. Vertical profiles of the mean vertical velocity and cloud ice, cloud water, rain water, and rimed cloud ice mixing ratio over the CCSs (a.b.c.e.f) and the mean profile of cloud water mixing ratio over the regions in moist clusters outside of CCSs (d).

412 A critical characteristic of tropical deep convection is the rapid intensification of
 413 precipitation once CWV has exceeded a critical value, which characterizes the effect of
 414 water vapor on the buoyancy of clouds through entrainment (Bretherton et al., 2004; Neelin
 415 et al., 2009; O. Peters & Neelin, 2006). We investigate the influence of pollution on this
 416 precipitation-CWV dependency. Analyses among all CCSs with a given CWV indicate
 417 that our simulations mimic the precipitation-CWV dependency seen in nature, with a
 418 rapid increase in precipitation (Fig. 8a) and updraft intensity (Fig. 8b-c) occurring above

419 a certain threshold in CWV. However, a distinct difference between the polluted run and
 420 the pristine one is that the threshold CWV that heralds the increase in convective in-
 421 tensity occurs at a lower CWV value (53 mm) than it does in the pristine run (57 mm).
 422 On the other hand, the highest CWV environment over CCSs in the pristine run (>65
 423 mm) is absent in the polluted run.

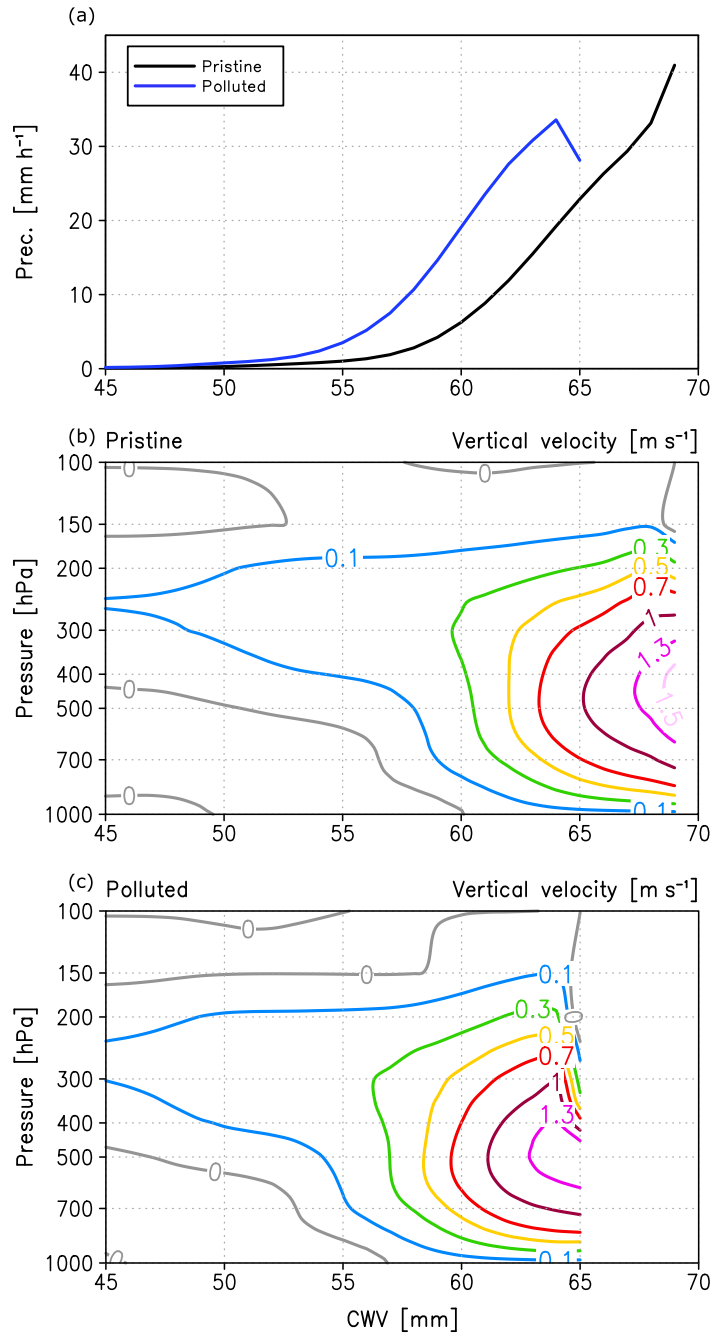


Figure 8. Precipitation intensity (a) and vertical velocity (b,c) within the CCSs conditional sampled by CWV from day 100 to 120.

424 Recall from Fig. 5a that mean CWV increases monotonically from dry regions to-
 425 ward moist clusters in both runs. We speculate that the spatial distribution of CCSs is
 426 a factor of the lower threshold CWV of rapid convection intensification in the polluted
 427 run. We apply the tracking analysis that links the CCSs overlapped in consecutive hourly
 428 outputs as a CCS track (Moseley et al., 2013) to find where CCSs start to develop. The
 429 tracked CCSs are classified into two categories according to how the CCS track initiates:
 430 emerging by itself and split from an existing CCS. Since our initiative is to identify the
 431 location where CCS triggering takes place, we only analyze the emerging tracks here.

432 Fig. 9 shows the distance-binned number of the emerging tracks with different present
 433 ages. The present age of a CCS is defined as the time difference between the present time
 434 step and the time step that the CCS emerged. In the polluted run, there are more tracks
 435 than the pristine run, and the maximum lifetime of the polluted tracks is longer. Tracks
 436 over dry regions have a shorter lifetime than tracks over moist clusters. The majority
 437 of young tracks (age < 12 hr) in the polluted run are located at regions closer to the edge
 438 than they are in the pristine run. The result verifies our speculation that the CCSs in
 439 the polluted run start to develop at regions closer to the edge with a lower CWV at which
 440 strong near-surface convergence takes place.

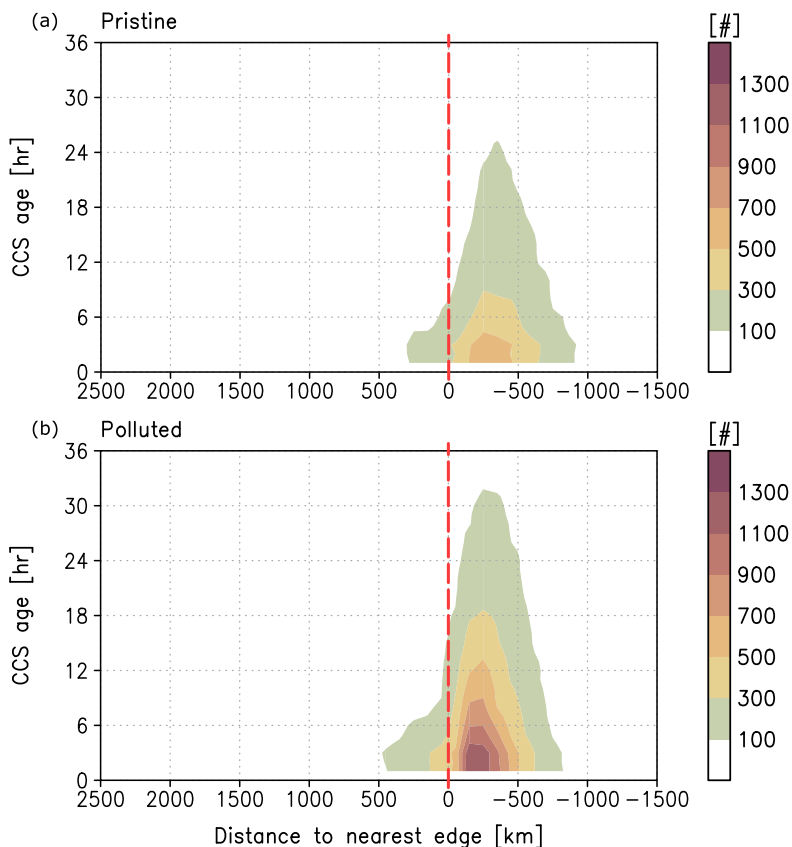


Figure 9. Number of CCSs with different present age (y-axis) conditionally sampled by the distance to the nearest edge in the pristine run (a) and the polluted run (b) from day 100 to 120.

441 Fig. 10a shows the probability distribution of the projected horizontal wind speed
 442 V_{in} at 1000 hPa over the regions of $0 < d < 50 \text{ km}$. Fig. 10b shows the probability

443 distribution of the estimated cold pool propagation velocity (Rotunno et al., 1988) over
 444 the CCSs

$$V_{cp} = \sqrt{2 \int_0^H -g \frac{\theta_\rho - \overline{\theta_\rho}(k)}{\overline{\theta_\rho}(k)} dz}, \quad (4)$$

445 where θ_ρ is the density potential temperature (K. A. Emanuel, 1994), k is the index of
 446 the moist cluster, overbars denote the average in k moist cluster but outside of CCSs,
 447 and H is the height of the cold pool given by the height at which θ_ρ is no longer smaller
 448 than $\overline{\theta_\rho}(k)$. As expected, the polluted run has the weaker V_{in} at 1000 hPa over the re-
 449 gions close to the edge. On the other hand, the impact of pollution on the distribution
 450 of estimated cold pool velocity is subtle. The distribution is slightly wider in the param-
 451 eter space in the polluted run. We note that the analyses here are column-based, whereas
 452 V_{in} and V_{cp} were calculated using the mean fields over the regions close to the edge of
 453 moist clusters in Windmiller and Hohenegger (2019). The difference in how the analy-
 454 sis is performed may influence the resulting V_{in} and V_{cp} individually. Our result high-
 455 lights that the weakening of near-surface inflow corroborates the closeness of the con-
 456 vection to the moist cluster edges in the polluted run, although the distribution of V_{in}
 457 does not approximately match the distribution of V_{cp} as shown in Fig. 8a in Windmiller
 458 and Hohenegger (2019).

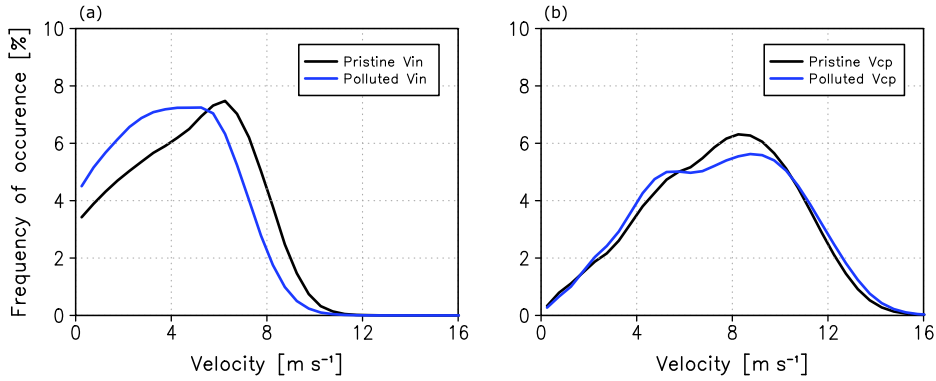


Figure 10. Probability distribution of V_{in} at 1000 hPa over the dry regions of $0 < d < 50$ km (a) and V_{cp} over the CCSs (b) from day 100 to 120.

459 Despite convection intensity starting to increase rapidly at a lower CWV in the pol-
 460 luted run, the two runs have the same increasing rate of convection intensity along with
 461 CWV. The CWV-binned precipitation intensities in the two runs can be collapsed by
 462 shifting the CWV by 4 mm. Why is the convection intensity limited in the polluted run
 463 (Fig. 7a)? We analyze the convective available potential energy (CAPE) for each moist
 464 cluster to identify the large-scale instability that constrains convection intensity. The CAPE
 465 is calculated as

$$CAPE_k = \int_{LFC}^{EL} B_k dz, \quad (5)$$

466 where k is the index of the moist cluster, LFC is the level of free convection, EL is the
 467 equilibrium level, and B_k is the buoyancy of the undiluted lifting parcel which is lifted
 468 adiabatically with freezing (J. M. Peters et al., 2022) from 2 m above ground level. The
 469 background environmental profile used for calculating B_k is the mean over regions within

470 k moist cluster but outside of CCSs. Fig. 11 shows the probability distribution of $CAPE$
 471 of moist clusters larger than 500 km of horizontal scale. The result indicates that moist
 472 clusters in the polluted run generally have less large-scale instability. The suspected re-
 473 duction in the upgradient energy transport by shallow circulation and the lower thresh-
 474 old CWV that may impede the accumulation of boundary layer moisture over moist clus-
 475 ters are both correlated to less $CAPE$ in the polluted run. Overall, the polluted run has
 476 a weaker convection intensity compared to the pristine run.

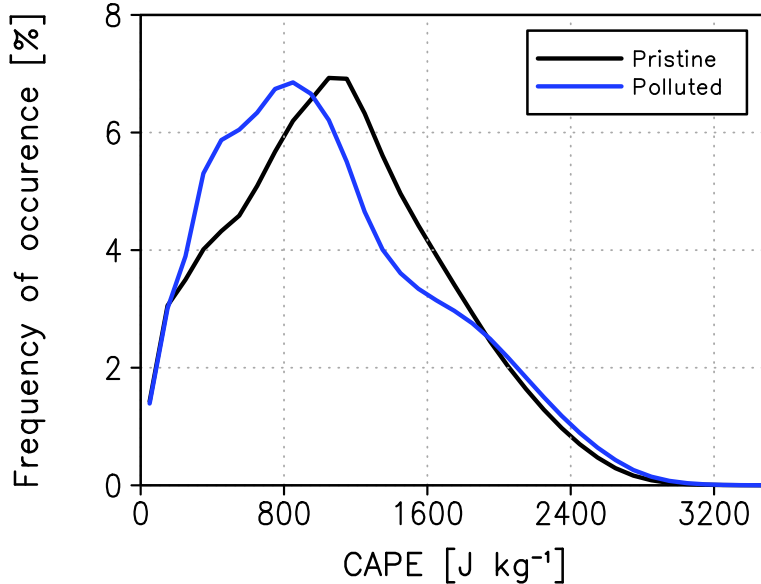


Figure 11. Moist cluster-based probability distribution of $CAPE$ from day 100 to 120.

477 4 Summary and Discussion

478 This study investigates the modulation of tropical convection-circulation interac-
 479 tion by enhanced CCN concentrations using a pair of non-rotating RCE simulations with
 480 the uniform and fixed SST of 300K of a global convection-permitting model. The model
 481 explicitly simulates the dynamic response of deep convection to the enhanced CCN con-
 482 centration and allows deep convection to interact with large-scale circulation without ar-
 483 tificial constraints of scale separation assumption and the geometry of the simulation do-
 484 main. The idealized setup of constant background aerosol concentration in the two simu-
 485 lations, namely the pristine run and the polluted run, is used to examine the changes
 486 in convection variability over space and the pattern of large-scale circulation with pol-
 487 lution. We analyze the difference between the pristine run and the polluted run at a sta-
 488 tistical equilibrium state of RCE in which the convective self-aggregation processes had
 489 occurred, resulting in an aggregated state maintained by large-scale circulations.

490 We found that pollution weakens large-scale circulations, including the deep cir-
 491 culation and the shallow circulation, and leads to a mean state with a lower degree of
 492 convective aggregation. Analysis of cold cloud systems tracking shows that deep convec-
 493 tive systems in the polluted run have notably more mid-level cloud water compared to
 494 the pristine run, and they preferably start to develop over regions close to the edge of
 495 moist clusters, contributing to the export of cloud water from moist clusters to dry re-
 496 gions. Pollution modulates how the diabatic processes that support or oppose convec-
 497 tive aggregation maintain the aggregated state at equilibrium, including the role of shal-

498 low circulation in the energy transport between moist clusters and dry regions. Over-
499 all, the analysis of precipitation-CWV dependency suggests that pollution facilitates the
500 development of deep convection in a drier environment but reduces the large-scale in-
501 stability and the convection intensity. Our results emphasize the importance of allow-
502 ing atmospheric phenomena to evolve continuously across spatial and temporal scales
503 in simulations when investigating the response of tropical convection to changes in cloud
504 microphysics. To our knowledge, this is the first study that simultaneously simulates the
505 response of deep convection to changes in cloud microphysics and postulates the impact
506 of pollution on the interaction between system-based tropical convection features and
507 large-scale circulation that develops without the limitation of horizontal scale.

508 Similarities between our results and previous studies of aerosol indirect effects on
509 tropical troposphere include weakened convection intensity (Beydoun & Hoose, 2019; Mor-
510 rison & Grabowski, 2011), atmospheric cooling (Nishant et al., 2019; Dagan, 2022), and
511 weakened convective aggregation (Beydoun & Hoose, 2019). However, there are contrast-
512 ing physical processes leading to the results. For example, enhanced high clouds amount
513 due to pollution leading to weaker tropospheric destabilization through radiative effects
514 are found critical to weakening convection in Morrison and Grabowski (2011) and Beydoun
515 and Hoose (2019). The polluted run has a less high cloud amount compared to the pris-
516 tine run in this study (Fig. 4 and Fig. 7). We suspect that the contrasting result in the
517 dependence of high clouds amount to pollution may be model dependent since the rep-
518 resentation of mixed-phase microphysical processes is believed to drive the large differ-
519 ence in tropical high clouds among the GCPMs (Nugent et al., 2022; Roh et al., 2021;
520 Turbeville et al., 2022). The equilibrium state analysis here provides a reference for stud-
521 ies aiming at finding causal relationships between physical processes. An investigation
522 focusing on the transition phase between different aggregated states due to pollution will
523 be carried out by the co-authors.

524 The current model runs at the horizontal resolution of around 15 km so that the
525 minimum scale of deep convection development is close to the scale of convective updraft
526 cores within an organized convective system (Houze, 2018). While we focus on the changes
527 in the multi-scale coupling processes associated with the response of tropical deep con-
528 vection to pollution, the study of van den Heever et al. (2011) suggested that aerosol in-
529 direct effects associated with tropical shallow clouds may offset or compensate for the
530 aerosol indirect effects associated with congestus and deep convection systems and vice
531 versa. We expect studies with the inclusion of the response of shallow convection to pol-
532 lution using the current research framework to come in the future. Parallel modeling ef-
533 forts to further depict the natural variability include heterogeneous aerosol perturbations,
534 cloud-aerosol interactions, air-sea interactions, and aerosol direct radiative effects.

535 A possible real-world manifestation of our result is the convection activity over the
536 Maritime Continent (MC) region. Past studies indicated that the large-scale organiza-
537 tion of convection in non-rotating RCE simulations and MJO-like (i.e., Madden-Julian
538 Oscillation; Madden & Julian, 1971) disturbance in rotating RCE simulations share the
539 same driving mechanism (i.e., cloud-radiation feedbacks) in which AIEs can be critical
540 (Arnold & Randall, 2015; Khairoutdinov & Emanuel, 2018). One of the leading theo-
541 ries of MJO propagation is that MJOs suffer from a barrier effect when they propagate
542 over the MC (Kim et al., 2014; Zhang & Ling, 2017). The development of convective sys-
543 tems over the ocean in the MC plays a crucial role in carrying the MJO signal (Ling et
544 al., 2019). As the MC is a major source of different types of aerosol around the globe
545 (Reid et al., 2012; Salinas et al., 2013; Shpund et al., 2019), evaluation of sub-seasonal
546 hindcasts spanning an active MJO event can be carried out to investigate the observed
547 relationship between the geographical distribution of convective systems and aerosol emis-
548 sion scenarios.

5 Open Research

A temporal snapshot of CWV, grid column distance to the nearest moist cluster edge, CCS, and the GrADS plotting scripts are available at <https://doi.org/10.6084/m9.figshare.22149617.v2>.

Acknowledgments

Chun-Yian Su and J. Peter's efforts were supported by National Science Foundation (NSF) grants AGS-1928666, AGS-1841674, and the Department of Energy Atmospheric System Research (DOE ASR) grant DE-SC0000246356. Chien-Ming Wu and Chun-Yian Su's efforts were supported by National Science and Technology Council of Taiwan grant 111-2111-M-002-012-NSTC. Wei-Ting Chen was supported by National Science and Technology Council of Taiwan grants NSTC112-2111-M-002-008, NSTC112-2111-M-002-015, and National Taiwan University grants NTU-112L7832 and NTU-112L7858. We thank Dr. Jen-Her Chen in Central Weather Bureau for his support of this work.

References

- Abbott, T. H., & Cronin, T. W. (2021, January). Aerosol invigoration of atmospheric convection through increases in humidity. *Science*, *371*(6524), 83–85. Retrieved from <https://doi.org/10.1126/science.abc5181> doi: 10.1126/science.abc5181
- Anber, U. M., Wang, S., Gentine, P., & Jensen, M. P. (2019, September). Probing the response of tropical deep convection to aerosol perturbations using idealized cloud-resolving simulations with parameterized large-scale dynamics. *Journal of the Atmospheric Sciences*, *76*(9), 2885–2897. Retrieved from <https://doi.org/10.1175/jas-d-18-0351.1> doi: 10.1175/jas-d-18-0351.1
- Andreae, M. O. (2009, January). Correlation between cloud condensation nuclei concentration and aerosol optical thickness in remote and polluted regions. *Atmospheric Chemistry and Physics*, *9*(2), 543–556. Retrieved from <https://doi.org/10.5194/acp-9-543-2009> doi: 10.5194/acp-9-543-2009
- Andreae, M. O., Rosenfeld, D., Artaxo, P., Costa, A. A., Frank, G. P., Longo, K. M., & Silva-Dias, M. A. F. (2004, February). Smoking rain clouds over the amazon. *Science*, *303*(5662), 1337–1342. Retrieved from <https://doi.org/10.1126/science.1092779> doi: 10.1126/science.1092779
- Arakawa, A. (2004, July). The cumulus parameterization problem: Past, present, and future. *Journal of Climate*, *17*(13), 2493–2525. Retrieved from [https://doi.org/10.1175/1520-0442\(2004\)017<2493:ratcpp>2.0.co;2](https://doi.org/10.1175/1520-0442(2004)017<2493:ratcpp>2.0.co;2) doi: 10.1175/1520-0442(2004)017(2493:ratcpp)2.0.co;2
- Arakawa, A., & Wu, C.-M. (2013, July). A unified representation of deep moist convection in numerical modeling of the atmosphere. part i. *Journal of the Atmospheric Sciences*, *70*(7), 1977–1992. Retrieved from <https://doi.org/10.1175/jas-d-12-0330.1> doi: 10.1175/jas-d-12-0330.1
- Arnold, N. P., & Putman, W. M. (2018, April). Nonrotating convective self-aggregation in a limited area AGCM. *Journal of Advances in Modeling Earth Systems*, *10*(4), 1029–1046. Retrieved from <https://doi.org/10.1002/2017ms001218> doi: 10.1002/2017ms001218
- Arnold, N. P., & Randall, D. A. (2015, October). Global-scale convective aggregation: Implications for the madden-julian oscillation. *Journal of Advances in Modeling Earth Systems*, *7*(4), 1499–1518. Retrieved from <https://doi.org/10.1002/2015ms000498> doi: 10.1002/2015ms000498
- Becker, T., Bretherton, C. S., Hohenegger, C., & Stevens, B. (2018, January). Estimating bulk entrainment with unaggregated and aggregated convection. *Geophysical Research Letters*, *45*(1), 455–462. Retrieved from <https://doi.org/10.1002/2017gl076640> doi: 10.1002/2017gl076640
- Beydoun, H., & Hoose, C. (2019, April). Aerosol-cloud-precipitation interactions

- 600 in the context of convective self-aggregation. *Journal of Advances in Modeling*
 601 *Earth Systems*, 11(4), 1066–1087. Retrieved from [https://doi.org/10.1029/](https://doi.org/10.1029/2018ms001523)
 602 [2018ms001523](https://doi.org/10.1029/2018ms001523) doi: 10.1029/2018ms001523
- 603 Bretherton, C. S., Blossey, P. N., & Khairoutdinov, M. (2005, December). An
 604 energy-balance analysis of deep convective self-aggregation above uniform SST.
 605 *Journal of the Atmospheric Sciences*, 62(12), 4273–4292. Retrieved from
 606 <https://doi.org/10.1175/jas3614.1> doi: 10.1175/jas3614.1
- 607 Bretherton, C. S., Peters, M. E., & Back, L. E. (2004, April). Relationships be-
 608 tween water vapor path and precipitation over the tropical oceans. *Jour-*
 609 *nal of Climate*, 17(7), 1517–1528. Retrieved from [https://doi.org/](https://doi.org/10.1175/1520-0442(2004)017<1517:rbwvpa>2.0.co;2)
 610 [10.1175/1520-0442\(2004\)017<1517:rbwvpa>2.0.co;2](https://doi.org/10.1175/1520-0442(2004)017<1517:rbwvpa>2.0.co;2)
 611 [doi: 10.1175/](https://doi.org/10.1175/1520-0442(2004)017(1517:rbwvpa)2.0.co;2)
 612 [1520-0442\(2004\)017\(1517:rbwvpa\)2.0.co;2](https://doi.org/10.1175/1520-0442(2004)017(1517:rbwvpa)2.0.co;2)
- 612 Caldwell, P. M., Terai, C. R., Hillman, B., Keen, N. D., Bogenschutz, P., Lin, W.,
 613 ... Zender, C. S. (2021, November). Convection-permitting simulations with
 614 the e3sm global atmosphere model. *Journal of Advances in Modeling Earth*
 615 *Systems*, 13(11). Retrieved from <https://doi.org/10.1029/2021ms002544>
 616 doi: 10.1029/2021ms002544
- 617 Chang, Y.-H., Chen, W.-T., Wu, C.-M., Moseley, C., & Wu, C.-C. (2021, Novem-
 618 ber). Tracking the influence of cloud condensation nuclei on summer diurnal
 619 precipitating systems over complex topography in taiwan. *Atmospheric Chem-*
 620 *istry and Physics*, 21(22), 16709–16725. Retrieved from [https://doi.org/](https://doi.org/10.5194/acp-21-16709-2021)
 621 [10.5194/acp-21-16709-2021](https://doi.org/10.5194/acp-21-16709-2021) doi: 10.5194/acp-21-16709-2021
- 622 Coppin, D., & Bony, S. (2015, December). Physical mechanisms controlling the
 623 initiation of convective self-aggregation in a general circulation model. *Jour-*
 624 *nal of Advances in Modeling Earth Systems*, 7(4), 2060–2078. Retrieved from
 625 <https://doi.org/10.1002/2015ms000571> doi: 10.1002/2015ms000571
- 626 Cronin, T. W., & Wing, A. A. (2017, December). Clouds, circulation, and climate
 627 sensitivity in a radiative-convective equilibrium channel model. *Journal of Ad-*
 628 *vances in Modeling Earth Systems*, 9(8), 2883–2905. Retrieved from [https://](https://doi.org/10.1002/2017ms001111)
 629 doi.org/10.1002/2017ms001111 doi: 10.1002/2017ms001111
- 630 Dagan, G. (2022, December). Equilibrium climate sensitivity increases with aerosol
 631 concentration due to changes in precipitation efficiency. *Atmospheric Chem-*
 632 *istry and Physics*, 22(24), 15767–15775. Retrieved from [https://doi.org/](https://doi.org/10.5194/acp-22-15767-2022)
 633 [10.5194/acp-22-15767-2022](https://doi.org/10.5194/acp-22-15767-2022) doi: 10.5194/acp-22-15767-2022
- 634 Dunion, J. P. (2011, February). Rewriting the climatology of the tropical north
 635 atlantic and caribbean sea atmosphere. *Journal of Climate*, 24(3), 893–
 636 908. Retrieved from <https://doi.org/10.1175/2010jcli3496.1> doi:
 637 [10.1175/2010jcli3496.1](https://doi.org/10.1175/2010jcli3496.1)
- 638 Emanuel, K., Wing, A. A., & Vincent, E. M. (2014, February). Radiative-
 639 convective instability. *Journal of Advances in Modeling Earth Systems*, 6(1),
 640 75–90. Retrieved from <https://doi.org/10.1002/2013ms000270> doi:
 641 [10.1002/2013ms000270](https://doi.org/10.1002/2013ms000270)
- 642 Emanuel, K. A. (1987, August). An air-sea interaction model of intraseasonal os-
 643 cillations in the tropics. *Journal of the Atmospheric Sciences*, 44(16), 2324–
 644 2340. Retrieved from [https://doi.org/10.1175/1520-0469\(1987\)044<2324:](https://doi.org/10.1175/1520-0469(1987)044<2324:aasimo>2.0.co;2)
 645 [aasimo>2.0.co;2](https://doi.org/10.1175/1520-0469(1987)044<2324:aasimo>2.0.co;2) doi: 10.1175/1520-0469(1987)044(2324:aasimo)2.0.co;2
- 646 Emanuel, K. A. (1994). *Atmospheric convection*. Oxford University Press, USA.
- 647 Fan, J., & Khain, A. (2021, January). Comments on “do ultrafine cloud condensa-
 648 tion nuclei invigorate deep convection?”. *Journal of the Atmospheric Sciences*,
 649 78(1), 329–339. Retrieved from <https://doi.org/10.1175/jas-d-20-0218.1>
 650 doi: 10.1175/jas-d-20-0218.1
- 651 Fan, J., Rosenfeld, D., Zhang, Y., Giangrande, S. E., Li, Z., Machado, L. A. T.,
 652 ... de Souza, R. A. F. (2018, January). Substantial convection and pre-
 653 cipitation enhancements by ultrafine aerosol particles. *Science*, 359(6374),
 654 411–418. Retrieved from <https://doi.org/10.1126/science.aan8461> doi:

- 10.1126/science.aan8461
- 655 Fan, J., Wang, Y., Rosenfeld, D., & Liu, X. (2016, October). Review of
 656 aerosol–cloud interactions: Mechanisms, significance, and challenges. *Jour-*
 657 *nal of the Atmospheric Sciences*, *73*(11), 4221–4252. Retrieved from
 658 <https://doi.org/10.1175/jas-d-16-0037.1> doi: 10.1175/jas-d-16-0037.1
- 659 Fan, J., Yuan, T., Comstock, J. M., Ghan, S., Khain, A., Leung, L. R., . . . Ovchin-
 660 nikov, M. (2009, November). Dominant role by vertical wind shear in regulat-
 661 ing aerosol effects on deep convective clouds. *Journal of Geophysical Research*,
 662 *114*(D22). Retrieved from <https://doi.org/10.1029/2009jd012352> doi:
 663 10.1029/2009jd012352
- 664 Feng, Z., Houze, R. A., Leung, L. R., Song, F., Hardin, J. C., Wang, J., . . .
 665 Homeyer, C. R. (2019, September). Spatiotemporal characteristics and
 666 large-scale environments of mesoscale convective systems east of the rocky
 667 mountains. *Journal of Climate*, *32*(21), 7303–7328. Retrieved from
 668 <https://doi.org/10.1175/jcli-d-19-0137.1> doi: 10.1175/jcli-d-19-0137.1
- 669 Feng, Z., Leung, L. R., Hardin, J., Terai, C. R., Song, F., & Caldwell, P. (2023,
 670 February). Mesoscale convective systems in DYAMOND global convection-
 671 permitting simulations. *Geophysical Research Letters*, *50*(4). Retrieved from
 672 <https://doi.org/10.1029/2022gl1102603> doi: 10.1029/2022gl1102603
- 673 Grabowski, W. W. (2018, October). Can the impact of aerosols on deep convec-
 674 tion be isolated from meteorological effects in atmospheric observations? *Jour-*
 675 *nal of the Atmospheric Sciences*, *75*(10), 3347–3363. Retrieved from [https://](https://doi.org/10.1175/jas-d-18-0105.1)
 676 doi.org/10.1175/jas-d-18-0105.1 doi: 10.1175/jas-d-18-0105.1
- 677 Grabowski, W. W., & Morrison, H. (2020, July). Do ultrafine cloud condensation
 678 nuclei invigorate deep convection? *Journal of the Atmospheric Sciences*, *77*(7),
 679 2567–2583. Retrieved from <https://doi.org/10.1175/jas-d-20-0012.1> doi:
 680 10.1175/jas-d-20-0012.1
- 681 Grabowski, W. W., & Morrison, H. (2021, January). Reply to “comments on ‘do ul-
 682 trafine cloud condensation nuclei invigorate deep convection?’”. *Journal of the*
 683 *Atmospheric Sciences*, *78*(1), 341–350. Retrieved from [https://doi.org/10](https://doi.org/10.1175/jas-d-20-0315.1)
 684 [.1175/jas-d-20-0315.1](https://doi.org/10.1175/jas-d-20-0315.1) doi: 10.1175/jas-d-20-0315.1
- 685 Hartmann, D. L., Moy, L. A., & Fu, Q. (2001, December). Tropical convection and
 686 the energy balance at the top of the atmosphere. *Journal of Climate*, *14*(24),
 687 4495–4511. Retrieved from [https://doi.org/10.1175/1520-0442\(2001\)](https://doi.org/10.1175/1520-0442(2001)014<4495:tcateb>2.0.co;2)
 688 [014<4495:tcateb>2.0.co;2](https://doi.org/10.1175/1520-0442(2001)014<4495:tcateb>2.0.co;2) doi: 10.1175/1520-0442(2001)014<4495:
 689 [tcateb>2.0.co;2](https://doi.org/10.1175/1520-0442(2001)014<4495:tcateb>2.0.co;2)
- 690 Hohenegger, C., Korn, P., Linardakis, L., Redler, R., Schnur, R., Adamidis, P., . . .
 691 Stevens, B. (2023, January). ICON-sapphire: simulating the components of
 692 the earth system and their interactions at kilometer and subkilometer scales.
 693 *Geoscientific Model Development*, *16*(2), 779–811. Retrieved from [https://](https://doi.org/10.5194/gmd-16-779-2023)
 694 doi.org/10.5194/gmd-16-779-2023 doi: 10.5194/gmd-16-779-2023
- 695 Holloway, C. E., & Woolnough, S. J. (2016, February). The sensitivity of convective
 696 aggregation to diabatic processes in idealized radiative-convective equilib-
 697 rium simulations. *Journal of Advances in Modeling Earth Systems*, *8*(1),
 698 166–195. Retrieved from <https://doi.org/10.1002/2015ms000511> doi:
 699 10.1002/2015ms000511
- 700 Houze, R. A. (2004, December). Mesoscale convective systems. *Reviews of Geo-*
 701 *physics*, *42*(4). Retrieved from <https://doi.org/10.1029/2004rg000150>
 702 doi: 10.1029/2004rg000150
- 703 Houze, R. A. (2018, January). 100 years of research on mesoscale convective sys-
 704 tems. *Meteorological Monographs*, *59*, 17.1–17.54. Retrieved from [https://doi](https://doi.org/10.1175/amsmonographs-d-18-0001.1)
 705 [.org/10.1175/amsmonographs-d-18-0001.1](https://doi.org/10.1175/amsmonographs-d-18-0001.1) doi: 10.1175/amsmonographs-d-
 706 18-0001.1
- 707 Igel, A. L., & van den Heever, S. C. (2021, August). Invigoration or enervation of
 708 convective clouds by aerosols? *Geophysical Research Letters*, *48*(16). Retrieved
 709

- 710 from <https://doi.org/10.1029/2021gl093804> doi: 10.1029/2021gl093804
- 711 Jeevanjee, N., & Romps, D. M. (2013, March). Convective self-aggregation, cold
712 pools, and domain size. *Geophysical Research Letters*, *40*(5), 994–998. Re-
713 trieved from <https://doi.org/10.1002/grl.50204> doi: 10.1002/grl.50204
- 714 Johnson, R. H., Rickenbach, T. M., Rutledge, S. A., Ciesielski, P. E., & Schu-
715 bert, W. H. (1999, August). Trimodal characteristics of tropical convec-
716 tion. *Journal of Climate*, *12*(8), 2397–2418. Retrieved from [https://doi.org/10.1175/1520-0442\(1999\)012<2397:tcotc>2.0.co;2](https://doi.org/10.1175/1520-0442(1999)012<2397:tcotc>2.0.co;2) doi:
717 10.1175/1520-0442(1999)012<2397:tcotc>2.0.co;2
- 718
- 719 Khain, A. P., BenMoshe, N., & Pokrovsky, A. (2008, June). Factors determining the
720 impact of aerosols on surface precipitation from clouds: An attempt at classifi-
721 cation. *Journal of the Atmospheric Sciences*, *65*(6), 1721–1748. Retrieved from
722 <https://doi.org/10.1175/2007jas2515.1> doi: 10.1175/2007jas2515.1
- 723 Khairoutdinov, M. F., & Emanuel, K. (2018, December). Intraseasonal variability in
724 a cloud-permitting near-global equatorial aquaplanet model. *Journal of the At-
725 mospheric Sciences*, *75*(12), 4337–4355. Retrieved from [https://doi.org/10.
726 .1175/jas-d-18-0152.1](https://doi.org/10.1175/jas-d-18-0152.1) doi: 10.1175/jas-d-18-0152.1
- 727 Kiladis, G. N., Wheeler, M. C., Haertel, P. T., Straub, K. H., & Roundy, P. E.
728 (2009, April). Convectively coupled equatorial waves. *Reviews of Geophysics*,
729 *47*(2). Retrieved from <https://doi.org/10.1029/2008rg000266> doi:
730 10.1029/2008rg000266
- 731 Kim, D., Kug, J.-S., & Sobel, A. H. (2014, January). Propagating versus non-
732 propagating madden–julian oscillation events. *Journal of Climate*, *27*(1),
733 111–125. Retrieved from <https://doi.org/10.1175/jcli-d-13-00084.1>
734 doi: 10.1175/jcli-d-13-00084.1
- 735 Koren, I., Feingold, G., & Remer, L. A. (2010, September). The invigoration
736 of deep convective clouds over the atlantic: aerosol effect, meteorology or
737 retrieval artifact? *Atmospheric Chemistry and Physics*, *10*(18), 8855–
738 8872. Retrieved from <https://doi.org/10.5194/acp-10-8855-2010> doi:
739 10.5194/acp-10-8855-2010
- 740 Koren, I., Martins, J. V., Remer, L. A., & Afargan, H. (2008, August). Smoke invig-
741 oration versus inhibition of clouds over the amazon. *Science*, *321*(5891), 946–
742 949. Retrieved from <https://doi.org/10.1126/science.1159185> doi: 10.
743 .1126/science.1159185
- 744 Lau, K.-H., & Lau, N.-C. (1990, September). Observed structure and prop-
745 agation characteristics of tropical summertime synoptic scale distur-
746 bances. *Monthly Weather Review*, *118*(9), 1888–1913. Retrieved from
747 [https://doi.org/10.1175/1520-0493\(1990\)118<1888:osapco>2.0.co;2](https://doi.org/10.1175/1520-0493(1990)118<1888:osapco>2.0.co;2)
748 doi: 10.1175/1520-0493(1990)118(1888:osapco)2.0.co;2
- 749 Lebo, Z. (2018, February). A numerical investigation of the potential effects of
750 aerosol-induced warming and updraft width and slope on updraft intensity
751 in deep convective clouds. *Journal of the Atmospheric Sciences*, *75*(2), 535–
752 554. Retrieved from <https://doi.org/10.1175/jas-d-16-0368.1> doi:
753 10.1175/jas-d-16-0368.1
- 754 Ling, J., Zhang, C., Joyce, R., ping Xie, P., & Chen, G. (2019, March). Possible role
755 of the diurnal cycle in land convection in the barrier effect on the MJO by the
756 maritime continent. *Geophysical Research Letters*, *46*(5), 3001–3011. Retrieved
757 from <https://doi.org/10.1029/2019gl081962> doi: 10.1029/2019gl081962
- 758 Madden, R. A., & Julian, P. R. (1971, July). Detection of a 40–50 day oscillation
759 in the zonal wind in the tropical pacific. *Journal of the Atmospheric Sciences*,
760 *28*(5), 702–708. Retrieved from [https://doi.org/10.1175/1520-0469\(1971\)
761 028<0702:doadoi>2.0.co;2](https://doi.org/10.1175/1520-0469(1971)028<0702:doadoi>2.0.co;2) doi: 10.1175/1520-0469(1971)028(0702:doadoi)2
762 .0.co;2
- 763 Manabe, S., & Strickler, R. F. (1964, July). Thermal equilibrium of the atmosphere
764 with a convective adjustment. *Journal of the Atmospheric Sciences*, *21*(4),

- 361–385. Retrieved from [https://doi.org/10.1175/1520-0469\(1964\)021<0361:teotaw>2.0.co;2](https://doi.org/10.1175/1520-0469(1964)021<0361:teotaw>2.0.co;2) doi: 10.1175/1520-0469(1964)021<0361:teotaw>2.0.co;2
- Mapes, B. E., Chung, E. S., Hannah, W. M., Masunaga, H., Wimmers, A. J., & Velden, C. S. (2018, January). The meandering margin of the meteorological moist tropics. *Geophysical Research Letters*, *45*(2), 1177–1184. Retrieved from <https://doi.org/10.1002/2017gl076440> doi: 10.1002/2017gl076440
- Matsugishi, S., & Satoh, M. (2022, May). Sensitivity of the horizontal scale of convective self-aggregation to sea surface temperature in radiative convective equilibrium experiments using a global nonhydrostatic model. *Journal of Advances in Modeling Earth Systems*, *14*(5). Retrieved from <https://doi.org/10.1029/2021ms002636> doi: 10.1029/2021ms002636
- Morrison, H., & Grabowski, W. W. (2007, August). Comparison of bulk and bin warm-rain microphysics models using a kinematic framework. *Journal of the Atmospheric Sciences*, *64*(8), 2839–2861. Retrieved from <https://doi.org/10.1175/jas3980> doi: 10.1175/jas3980
- Morrison, H., & Grabowski, W. W. (2008, March). Modeling supersaturation and subgrid-scale mixing with two-moment bulk warm microphysics. *Journal of the Atmospheric Sciences*, *65*(3), 792–812. Retrieved from <https://doi.org/10.1175/2007jas2374.1> doi: 10.1175/2007jas2374.1
- Morrison, H., & Grabowski, W. W. (2011, October). Cloud-system resolving model simulations of aerosol indirect effects on tropical deep convection and its thermodynamic environment. *Atmospheric Chemistry and Physics*, *11*(20), 10503–10523. Retrieved from <https://doi.org/10.5194/acp-11-10503-2011> doi: 10.5194/acp-11-10503-2011
- Morrison, H., & Milbrandt, J. A. (2015, January). Parameterization of cloud microphysics based on the prediction of bulk ice particle properties. part i: Scheme description and idealized tests. *Journal of the Atmospheric Sciences*, *72*(1), 287–311. Retrieved from <https://doi.org/10.1175/jas-d-14-0065.1> doi: 10.1175/jas-d-14-0065.1
- Moseley, C., Berg, P., & Haerter, J. O. (2013, dec). Probing the precipitation life cycle by iterative rain cell tracking. *Journal of Geophysical Research: Atmospheres*, *118*(24), 13,361–13,370. Retrieved from <https://doi.org/10.1002/2013jd020868> doi: 10.1002/2013jd020868
- Muller, C., Yang, D., Craig, G., Cronin, T., Fildier, B., Haerter, J. O., ... Sherwood, S. C. (2022, January). Spontaneous aggregation of convective storms. *Annual Review of Fluid Mechanics*, *54*(1), 133–157. Retrieved from <https://doi.org/10.1146/annurev-fluid-022421-011319> doi: 10.1146/annurev-fluid-022421-011319
- Muller, C. J., & Held, I. M. (2012, August). Detailed investigation of the self-aggregation of convection in cloud-resolving simulations. *Journal of the Atmospheric Sciences*, *69*(8), 2551–2565. Retrieved from <https://doi.org/10.1175/jas-d-11-0257.1> doi: 10.1175/jas-d-11-0257.1
- Neelin, J. D., & Held, I. M. (1987, January). Modeling tropical convergence based on the moist static energy budget. *Monthly Weather Review*, *115*(1), 3–12. Retrieved from [https://doi.org/10.1175/1520-0493\(1987\)115<0003:mtcbot>2.0.co;2](https://doi.org/10.1175/1520-0493(1987)115<0003:mtcbot>2.0.co;2) doi: 10.1175/1520-0493(1987)115<0003:mtcbot>2.0.co;2
- Neelin, J. D., Peters, O., & Hales, K. (2009, August). The transition to strong convection. *Journal of the Atmospheric Sciences*, *66*(8), 2367–2384. Retrieved from <https://doi.org/10.1175/2009jas2962.1> doi: 10.1175/2009jas2962.1
- Nishant, N., & Sherwood, S. C. (2017, June). A cloud-resolving model study of aerosol-cloud correlation in a pristine maritime environment. *Geophysical Research Letters*, *44*(11), 5774–5781. Retrieved from <https://doi.org/10.1002/2017gl073267> doi: 10.1002/2017gl073267

- 820 Nishant, N., Sherwood, S. C., & Geoffroy, O. (2019, September). Aerosol-induced
821 modification of organised convection and top-of-atmosphere radiation. *npj*
822 *Climate and Atmospheric Science*, 2(1). Retrieved from [https://doi.org/](https://doi.org/10.1038/s41612-019-0089-1)
823 [10.1038/s41612-019-0089-1](https://doi.org/10.1038/s41612-019-0089-1) doi: 10.1038/s41612-019-0089-1
- 824 Niu, F., & Li, Z. (2012, September). Systematic variations of cloud top tempera-
825 ture and precipitation rate with aerosols over the global tropics. *Atmospheric*
826 *Chemistry and Physics*, 12(18), 8491–8498. Retrieved from [https://doi.org/](https://doi.org/10.5194/acp-12-8491-2012)
827 [10.5194/acp-12-8491-2012](https://doi.org/10.5194/acp-12-8491-2012) doi: 10.5194/acp-12-8491-2012
- 828 Nugent, J. M., Turbeville, S. M., Bretherton, C. S., Blossey, P. N., & Ackerman,
829 T. P. (2022, February). Tropical cirrus in global storm-resolving models:
830 1. role of deep convection. *Earth and Space Science*, 9(2). Retrieved from
831 <https://doi.org/10.1029/2021ea001965> doi: 10.1029/2021ea001965
- 832 Pan, Z., Rosenfeld, D., Zhu, Y., Mao, F., Gong, W., Zang, L., & Lu, X. (2021,
833 May). Observational quantification of aerosol invigoration for deep convective
834 cloud lifecycle properties based on geostationary satellite. *Journal of Geo-*
835 *physical Research: Atmospheres*, 126(9). Retrieved from [https://doi.org/](https://doi.org/10.1029/2020jd034275)
836 [10.1029/2020jd034275](https://doi.org/10.1029/2020jd034275) doi: 10.1029/2020jd034275
- 837 Patrizio, C. R., & Randall, D. A. (2019, July). Sensitivity of convective self-
838 aggregation to domain size. *Journal of Advances in Modeling Earth Systems*,
839 11(7), 1995–2019. Retrieved from <https://doi.org/10.1029/2019ms001672>
840 doi: 10.1029/2019ms001672
- 841 Pendergrass, A. G., Reed, K. A., & Medeiros, B. (2016, November). The link be-
842 tween extreme precipitation and convective organization in a warming climate:
843 Global radiative-convective equilibrium simulations. *Geophysical Research Let-*
844 *ters*, 43(21). Retrieved from <https://doi.org/10.1002/2016gl071285> doi:
845 10.1002/2016gl071285
- 846 Peters, J. M., Lebo, Z. J., Chavas, D. R., & Su, C.-Y. (2023, June). Entrain-
847 ment makes pollution more likely to weaken deep convective updrafts than
848 invigorate them. *Geophysical Research Letters*, 50(12). Retrieved from
849 <https://doi.org/10.1029/2023gl1103314> doi: 10.1029/2023gl1103314
- 850 Peters, J. M., Mulholland, J. P., & Chavas, D. R. (2022, March). Generalized lapse
851 rate formulas for use in entraining CAPE calculations. *Journal of the Atmo-*
852 *spheric Sciences*, 79(3), 815–836. Retrieved from [https://doi.org/10.1175/](https://doi.org/10.1175/jas-d-21-0118.1)
853 [jas-d-21-0118.1](https://doi.org/10.1175/jas-d-21-0118.1) doi: 10.1175/jas-d-21-0118.1
- 854 Peters, O., & Neelin, J. D. (2006, May). Critical phenomena in atmospheric precip-
855 itation. *Nature Physics*, 2(6), 393–396. Retrieved from [https://doi.org/10](https://doi.org/10.1038/nphys314)
856 [.1038/nphys314](https://doi.org/10.1038/nphys314) doi: 10.1038/nphys314
- 857 Popke, D., Stevens, B., & Voigt, A. (2013, January). Climate and climate change
858 in a radiative-convective equilibrium version of ECHAM6. *Journal of Advances*
859 *in Modeling Earth Systems*, 5(1), 1–14. Retrieved from [https://doi.org/10](https://doi.org/10.1029/2012ms000191)
860 [.1029/2012ms000191](https://doi.org/10.1029/2012ms000191) doi: 10.1029/2012ms000191
- 861 Posselt, D. J., van den Heever, S. C., & Stephens, G. L. (2008, April). Tri-
862 modal cloudiness and tropical stable layers in simulations of radiative con-
863 vective equilibrium. *Geophysical Research Letters*, 35(8). Retrieved from
864 <https://doi.org/10.1029/2007gl033029> doi: 10.1029/2007gl033029
- 865 Reid, J. S., Xian, P., Hyer, E. J., Flatau, M. K., Ramirez, E. M., Turk, F. J., ...
866 Maloney, E. D. (2012, February). Multi-scale meteorological conceptual
867 analysis of observed active fire hotspot activity and smoke optical depth in
868 the maritime continent. *Atmospheric Chemistry and Physics*, 12(4), 2117–
869 2147. Retrieved from <https://doi.org/10.5194/acp-12-2117-2012> doi:
870 10.5194/acp-12-2117-2012
- 871 Roh, W., Satoh, M., & Hohenegger, C. (2021). Intercomparison of cloud properties
872 in DYAMOND simulations over the atlantic ocean. *Journal of the Meteorolog-*
873 *ical Society of Japan. Ser. II*, 99(6), 1439–1451. Retrieved from [https://doi](https://doi.org/10.2151/jmsj.2021-070)
874 [.org/10.2151/jmsj.2021-070](https://doi.org/10.2151/jmsj.2021-070) doi: 10.2151/jmsj.2021-070

- 875 Romps, D. M., Latimer, K., Zhu, Q., Jurkat-Witschas, T., Mahnke, C., Prab-
876 hakaran, T., ... Wendisch, M. (2023, January). Air pollution unable to
877 intensify storms via warm-phase invigoration. *Geophysical Research Letters*,
878 *50*(2). Retrieved from <https://doi.org/10.1029/2022gl1100409> doi:
879 10.1029/2022gl1100409
- 880 Rosenfeld, D. (1999, October). TRMM observed first direct evidence of smoke
881 from forest fires inhibiting rainfall. *Geophysical Research Letters*, *26*(20),
882 3105–3108. Retrieved from <https://doi.org/10.1029/1999gl1006066> doi:
883 10.1029/1999gl1006066
- 884 Rosenfeld, D., Lohmann, U., Raga, G. B., O'Dowd, C. D., Kulmala, M., Fuzzi,
885 S., ... Andreae, M. O. (2008, September). Flood or drought: How do
886 aerosols affect precipitation? *Science*, *321*(5894), 1309–1313. Retrieved from
887 <https://doi.org/10.1126/science.1160606> doi: 10.1126/science.1160606
- 888 Rotunno, R., Klemp, J. B., & Weisman, M. L. (1988, February). A theory for
889 strong, long-lived squall lines. *Journal of the Atmospheric Sciences*, *45*(3),
890 463–485. Retrieved from [https://doi.org/10.1175/1520-0469\(1988\)
891 045<0463:atfsl1>2.0.co;2](https://doi.org/10.1175/1520-0469(1988)045<0463:atfsl1>2.0.co;2) doi: 10.1175/1520-0469(1988)045<0463:
892 atfsl1>2.0.co;2
- 893 Salinas, S. V., Chew, B. N., Miettinen, J., Campbell, J. R., Welton, E. J., Reid,
894 J. S., ... Liew, S. C. (2013, March). Physical and optical characteristics of
895 the october 2010 haze event over singapore: A photometric and lidar analy-
896 sis. *Atmospheric Research*, *122*, 555–570. Retrieved from [https://doi.org/
897 10.1016/j.atmosres.2012.05.021](https://doi.org/10.1016/j.atmosres.2012.05.021) doi: 10.1016/j.atmosres.2012.05.021
- 898 Shpund, J., Khain, A., & Rosenfeld, D. (2019, August). Effects of sea spray on mi-
899 crophysics and intensity of deep convective clouds under strong winds. *Jour-
900 nal of Geophysical Research: Atmospheres*, *124*(16), 9484–9509. Retrieved from
901 <https://doi.org/10.1029/2018jd029893> doi: 10.1029/2018jd029893
- 902 Singh, M. S., & O'Gorman, P. A. (2013, August). Influence of entrainment
903 on the thermal stratification in simulations of radiative-convective equilib-
904 rium. *Geophysical Research Letters*, *40*(16), 4398–4403. Retrieved from
905 <https://doi.org/10.1002/grl.50796> doi: 10.1002/grl.50796
- 906 Singh, M. S., & O'Gorman, P. A. (2015, June). Increases in moist-convective up-
907 draught velocities with warming in radiative-convective equilibrium. *Quarterly
908 Journal of the Royal Meteorological Society*, *141*(692), 2828–2838. Retrieved
909 from <https://doi.org/10.1002/qj.2567> doi: 10.1002/qj.2567
- 910 Sobel, A. H., Nilsson, J., & Polvani, L. M. (2001, December). The weak temper-
911 ature gradient approximation and balanced tropical moisture waves. *Journal
912 of the Atmospheric Sciences*, *58*(23), 3650–3665. Retrieved from [https://doi
913 .org/10.1175/1520-0469\(2001\)058<3650:twtgaa>2.0.co;2](https://doi.org/10.1175/1520-0469(2001)058<3650:twtgaa>2.0.co;2) doi: 10.1175/
914 1520-0469(2001)058(3650:twtgaa)2.0.co;2
- 915 Stevens, B., Satoh, M., Auger, L., Biercamp, J., Bretherton, C. S., Chen, X., ...
916 Zhou, L. (2019, September). DYAMOND: the DYnamics of the atmospheric
917 general circulation modeled on non-hydrostatic domains. *Progress in Earth
918 and Planetary Science*, *6*(1). Retrieved from [https://doi.org/10.1186/
919 s40645-019-0304-z](https://doi.org/10.1186/s40645-019-0304-z) doi: 10.1186/s40645-019-0304-z
- 920 Storer, R. L., & van den Heever, S. C. (2013, February). Microphysical processes
921 evident in aerosol forcing of tropical deep convective clouds. *Journal of the
922 Atmospheric Sciences*, *70*(2), 430–446. Retrieved from [https://doi.org/
923 10.1175/jas-d-12-076.1](https://doi.org/10.1175/jas-d-12-076.1) doi: 10.1175/jas-d-12-076.1
- 924 Storer, R. L., van den Heever, S. C., & L'Ecuyer, T. S. (2014, April). Observations
925 of aerosol-induced convective invigoration in the tropical east atlantic. *Jour-
926 nal of Geophysical Research: Atmospheres*, *119*(7), 3963–3975. Retrieved from
927 <https://doi.org/10.1002/2013jd020272> doi: 10.1002/2013jd020272
- 928 Su, C.-Y., Chen, W.-T., Wu, C.-M., & Ma, H.-Y. (2022). Object-based evaluation
929 of tropical precipitation systems in DYAMOND simulations over the maritime

- continent. *Journal of the Meteorological Society of Japan. Ser. II*, 100(4), 647–659. Retrieved from <https://doi.org/10.2151/jmsj.2022-033> doi: 10.2151/jmsj.2022-033
- Su, C.-Y., Wu, C.-M., Chen, W.-T., & Chen, J.-H. (2021a, July). The effects of the unified parameterization in the CWBGFS: the diurnal cycle of precipitation over land in the maritime continent. *Climate Dynamics*, 58(1-2), 223–233. Retrieved from <https://doi.org/10.1007/s00382-021-05899-2> doi: 10.1007/s00382-021-05899-2
- Su, C.-Y., Wu, C.-M., Chen, W.-T., & Chen, J.-H. (2021b, October). Implementation of the unified representation of deep moist convection in the CWBGFS. *Monthly Weather Review*, 149(10), 3525–3539. Retrieved from <https://doi.org/10.1175/mwr-d-21-0067.1> doi: 10.1175/mwr-d-21-0067.1
- Tao, W.-K., Chen, J.-P., Li, Z., Wang, C., & Zhang, C. (2012, April). Impact of aerosols on convective clouds and precipitation. *Reviews of Geophysics*, 50(2). Retrieved from <https://doi.org/10.1029/2011rg000369> doi: 10.1029/2011rg000369
- Tomassini, L. (2020, August). The interaction between moist convection and the atmospheric circulation in the tropics. *Bulletin of the American Meteorological Society*, 101(8), E1378–E1396. Retrieved from <https://doi.org/10.1175/bams-d-19-0180.1> doi: 10.1175/bams-d-19-0180.1
- Tsai, W.-M., & Wu, C.-M. (2017, September). The environment of aggregated deep convection. *Journal of Advances in Modeling Earth Systems*, 9(5), 2061–2078. Retrieved from <https://doi.org/10.1002/2017ms000967> doi: 10.1002/2017ms000967
- Turbeville, S. M., Nugent, J. M., Ackerman, T. P., Bretherton, C. S., & Blossey, P. N. (2022, February). Tropical cirrus in global storm-resolving models: 2. cirrus life cycle and top-of-atmosphere radiative fluxes. *Earth and Space Science*, 9(2). Retrieved from <https://doi.org/10.1029/2021ea001978> doi: 10.1029/2021ea001978
- van den Heever, S. C., & Cotton, W. R. (2007, June). Urban aerosol impacts on downwind convective storms. *Journal of Applied Meteorology and Climatology*, 46(6), 828–850. Retrieved from <https://doi.org/10.1175/jam2492.1> doi: 10.1175/jam2492.1
- van den Heever, S. C., Stephens, G. L., & Wood, N. B. (2011, April). Aerosol indirect effects on tropical convection characteristics under conditions of radiative–convective equilibrium. *Journal of the Atmospheric Sciences*, 68(4), 699–718. Retrieved from <https://doi.org/10.1175/2010jas3603.1> doi: 10.1175/2010jas3603.1
- Varble, A. (2018, April). Erroneous attribution of deep convective invigoration to aerosol concentration. *Journal of the Atmospheric Sciences*, 75(4), 1351–1368. Retrieved from <https://doi.org/10.1175/jas-d-17-0217.1> doi: 10.1175/jas-d-17-0217.1
- Windmiller, J. M., & Hohenegger, C. (2019, December). Convection on the edge. *Journal of Advances in Modeling Earth Systems*, 11(12), 3959–3972. Retrieved from <https://doi.org/10.1029/2019ms001820> doi: 10.1029/2019ms001820
- Wing, A. A., Emanuel, K., Holloway, C. E., & Muller, C. (2017, February). Convective self-aggregation in numerical simulations: A review. *Surveys in Geophysics*, 38(6), 1173–1197. Retrieved from <https://doi.org/10.1007/s10712-017-9408-4> doi: 10.1007/s10712-017-9408-4
- Wing, A. A., & Emanuel, K. A. (2014, February). Physical mechanisms controlling self-aggregation of convection in idealized numerical modeling simulations. *Journal of Advances in Modeling Earth Systems*, 6(1), 59–74. Retrieved from <https://doi.org/10.1002/2013ms000269> doi: 10.1002/2013ms000269
- Wing, A. A., Reed, K. A., Satoh, M., Stevens, B., Bony, S., & Ohno, T. (2018, March). Radiative–convective equilibrium model intercomparison project.

- 985 *Geoscientific Model Development*, 11(2), 793–813. Retrieved from [https://](https://doi.org/10.5194/gmd-11-793-2018)
986 doi.org/10.5194/gmd-11-793-2018 doi: 10.5194/gmd-11-793-2018
- 987 Wing, A. A., Stauffer, C. L., Becker, T., Reed, K. A., Ahn, M.-S., Arnold, N. P.,
988 ... Zhao, M. (2020, September). Clouds and convective self-aggregation
989 in a multimodel ensemble of radiative-convective equilibrium simulations.
990 *Journal of Advances in Modeling Earth Systems*, 12(9). Retrieved from
991 <https://doi.org/10.1029/2020ms002138> doi: 10.1029/2020ms002138
- 992 Wu, C.-M., & Arakawa, A. (2014, May). A unified representation of deep moist con-
993 vection in numerical modeling of the atmosphere. part II. *Journal of the At-*
994 *mospheric Sciences*, 71(6), 2089–2103. Retrieved from [https://doi.org/10](https://doi.org/10.1175/jas-d-13-0382.1)
995 [.1175/jas-d-13-0382.1](https://doi.org/10.1175/jas-d-13-0382.1) doi: 10.1175/jas-d-13-0382.1
- 996 Yanase, T., Nishizawa, S., Miura, H., & Tomita, H. (2022, September). Character-
997 istic form and distance in high-level hierarchical structure of self-aggregated
998 clouds in radiative-convective equilibrium. *Geophysical Research Letters*,
999 49(18). Retrieved from <https://doi.org/10.1029/2022gl1100000> doi:
1000 10.1029/2022gl1100000
- 1001 Yang, G.-Y., & Slingo, J. (2001, April). The diurnal cycle in the tropics.
1002 *Monthly Weather Review*, 129(4), 784–801. Retrieved from [https://](https://doi.org/10.1175/1520-0493(2001)129<0784:tdcitt>2.0.co;2)
1003 [doi.org/10.1175/1520-0493\(2001\)129<0784:tdcitt>2.0.co;2](https://doi.org/10.1175/1520-0493(2001)129<0784:tdcitt>2.0.co;2) doi:
1004 10.1175/1520-0493(2001)129<0784:tdcitt>2.0.co;2
- 1005 Zhang, C., & Ling, J. (2017, May). Barrier effect of the indo-pacific maritime con-
1006 tinent on the MJO: Perspectives from tracking MJO precipitation. *Journal of*
1007 *Climate*, 30(9), 3439–3459. Retrieved from [https://doi.org/10.1175/jcli](https://doi.org/10.1175/jcli-d-16-0614.1)
1008 [-d-16-0614.1](https://doi.org/10.1175/jcli-d-16-0614.1) doi: 10.1175/jcli-d-16-0614.1